1. Geological background and sample descriptions
2. Grain size distributions
3. FTIR and identification of hydrated samples
4. EPMA and determination of post-entrapment crystallisation
5. SIMS analysis
6. Post-entrapment modification & identification of unrepresentative melt inclusions

Geological background and sample descriptions

Secondary ion mass spectrometry (SIMS) was performed on 14 samples (T1), collected from 5 edifices (T2) within the Torfajökull central volcanic complex in South Iceland. The five subglacial rhyolitic edifices demonstrate a wide variety of sizes, morphologies, and lithofacies (T2, F1-5) which are thought to reflect contrasting eruptive styles. Many previous authors have speculated reasons for the contrasting eruptive behaviour of these edifices (T2) but these conjectural models (Furnes et al., 1980; McGarvie et al., 2007; Tuffen et al., 2007; Tuffen et al., 2008; Stevenson et al., 2011) lack pre-eruptive volatile data.

Table DR1: A brief summary of the samples collected, the sampling locations and the analytical work done on each

EPMA	no	yes	yes	yes	yes	yes	yes	yes	yes	yes	no	yes	yes	yes	no	no	no	no	no
FTIR	yes	n.a.	yes	yes	n.a.	n.a.	yes	n.a.	yes	yes	yes	yes	n.a.	yes	yes	yes	yes	yes	yes
SIMS	yes	no	yes	yes	no	no	yes	no	yes	yes	yes	yes	no	yes	yes	yes	yes	yes	yes
sample description	obsidian	obsidian	obsidian	obsidian	obsidian	obsidian	obsidian	v.p. obsidian	obsidian	obsidian	Pumiceous clast	obsidian	Tran.	obsidian	obsidian	obsidian	v.p. ob clast	obsidian clast	obsidian clast
Locality description	Columns near the summit	large intrusive sill-like lava body	lava lobe	lava lobe	lava lobe	columnar jointed dyke-like lava body	columnar jointed dyke	lava lobe	lava lobe	lava lobe	crudely bedded ash deposit	obsidian sheet	obsidian sheet	poorly exposed mound of dense obsidian	conduit	Easter Plateau lava cap	fragmental deposit	fragmental deposit	top of subglacial fragmental pile
Reference facies*	/	cjl[a]	A[a]	B[a]	A[a]	cjl[a]	cjl[a]	B[a]	A[a]	cj[b]	cba[b]	os[b]	os[b]	pl*[b]	B[c]	E[c]	a[c]	a[c]	/
Elevation (m)	1090	671	710	620	880	862	937	793	860	715	697	682	682	710	1174	888	-	870	1039
GPS	N 64 00 36.5, W 019 23 46.1	N 63 58 49.5, W 019 03 21.5	N 63 58 58.7, W 019 03 43.6	N 63 59 03.8, W 019 03 50.6	N 63 58 37.6, W 019 04 21.5	N 63 58 39.5, W 019 03 55.4	N 63 58 35.3, W 019 04 08.1	N 63 58 39.4, W 019 04 44.6	N 63 58 36.9, W 019 04 26.5	N 64 00 22.6, W019 19 51.5	N 64 00 32.2, W019 19 10.7	N 64 00 45.3, W019 19 31.0	N 64 00 45.3, W019 19 31.0	N 64 00 55.8, W019 19 40.1	N 63 58 59.3, W019 24 27.3	N 63 57 50.3, W019 24 34.8	-	N 63 58 52.8, W019 23 23.3	N 63 59 52.6, W019 23 44.0
Sample name	A1a	B2	J2b	J3	J5	J10	J11	L6c	L8bott	D1	D7b	D13a	D13b	D22	R7	R13	R20	R24a	S1e
Location	Angel Peak	Bláhnúkur								Dalakvísl					SE Rauðfossafjöll				NW Rauðfossafjöll
Location	Angel Peak	Bláhnúkur								Dalakvísl					SE Rauðfossafjöll				NW Rauðfossafjöll

- = No GPS information; *= The lithofacies group from which the sample was collected according to the geological map stated by the superscript where [a] = (Tuffen et al., 2001): cjl = "columnar jointed lava"; A = "lava lobe-breccia A"; B = "breccia B" [b] = (Tuffen et al., 2008): cj = "columnar jointed lava lobes"; cba = "crudely bedded ash"; os = "massive breccia with obsidian sheets"; pl* = a non-perlitised sample from "perlitised lava" [c] = (Tuffen et al., 2002a): B = "lava B"; E = "lava E"; a = "rhyolitic ash"; / = No reference facies i.e. these edifices have not been previously described in the literature; Lava lobe = conical-to-irregularly shaped, 5-10 m long protruding lava body (Tuffen et al., 2001); Obsidian sheet = elongated lava body (1-20 m long, 0.5-1 m thick) that have obsidian cores and pumiceous carapaces (Tuffen et al., 2008); v.p. = variably perlitised; tran. = Transitional between obsidian and pumice; n.a. = not applicable i.e. FTIR data does exist but it is beyond the scope of this paper

Table DR2: A summary of the sizes, morphologies, lithofacies and inferred eruptive behaviour for the five edifices featured in this study

Fig.	1	2	3	4	5
Existing model for style		Open-system degassing?[d] Low initial water content?[f] High confining pressure?[g]	Increasing confining pressure due to cavity filling?[g,h] De-pressuriation associated with a jökulhlaup?[a]	Low confining pressure?[g] High initial water content?[k]	
Inferred eruptive style	effusive	Effusive[b,c]	mixed: effusive-explosive[h]	Explosive[i]	explosive
Inferred ice surface elevation / m **(ice thickness / m)**[†]	1120[a] (120)	1000[e] (400)	1000[a] (330)	1090[j] (290)	1090[j] (290)
Eruptive environment	Entirely subglacial	Entirely subglacial[b,c,]	Entirely subglacial[h¥]	Emergent[j]	Emergent
Dominant lithofacies	Quench hyaloclastite and massive columnar jointed obsidian	lobe-bearing hyaloclastite[b,c,d]	A diverse range, from lava lobes to ash pumice breccia[h]	Fragmental deposits capped by subaerial lava[i]	Fragmental deposits capped by subaerial lava
Morphology	conical mound	pryamidal mound	double mound	steep-sided flat topped tuya[i]	steep-sided flat topped tuya
Volume / km^3	< 0.1	< 0.1[b]	<0.2[h]	~1[j]	~1
Height / m	100	350*	100	400	400
Part of ring fracture unit?	Yes	No	Yes	Yes	Yes
Edifice	**Angel Peak**	**Bláhnúkur**	**Dalakvísl**	**SE Rauðfossafjöll**	**NW Rauðfossafjöll**

* = the edifice height is 350 m but the eruptive deposits provide just a 50 m thick veneer over pre-existing topography

¥ = lithofacies support an entirely subglacial setting, although perlitised lava at the summit could indicate the initiation of a subaerial lava cap (Tuffen et al., 2008).

† = These thicknesses do not take into account ice cauldron depths which could be up to 150 m deep (Guðmundsson et al., 2004)

a = (Owen et al., unpublished results); b= (Tuffen et al., 2001); c = (Tuffen et al., 2002b); d = (Furnes et al., 1980); e= (Owen et al., 2012); f = (Stevenson et al., 2011); g = (Tuffen et al., 2007); h = (Tuffen et al., 2008); i = (Tuffen et al., 2002a); k = (McGarvie et al., 2006); k = (McGarvie et al., 2007)

Figure DR1: typical deposits from Angel Peak (a) overview (b) columnar jointed obsidian (c) small, vesicular, highly fractured lava bodies

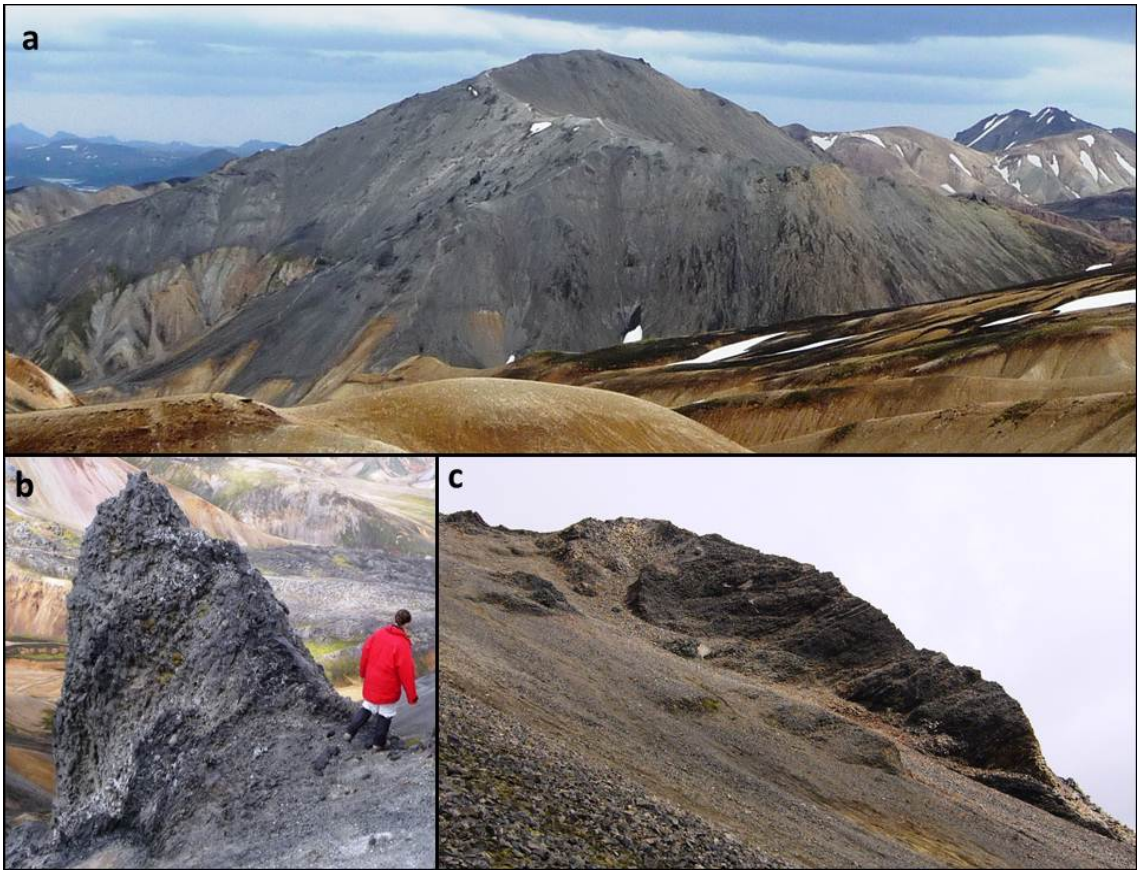

F2: typical deposits from Bláhnúkur (a) overview (b) lava lobe (c) columnar jointed dyke

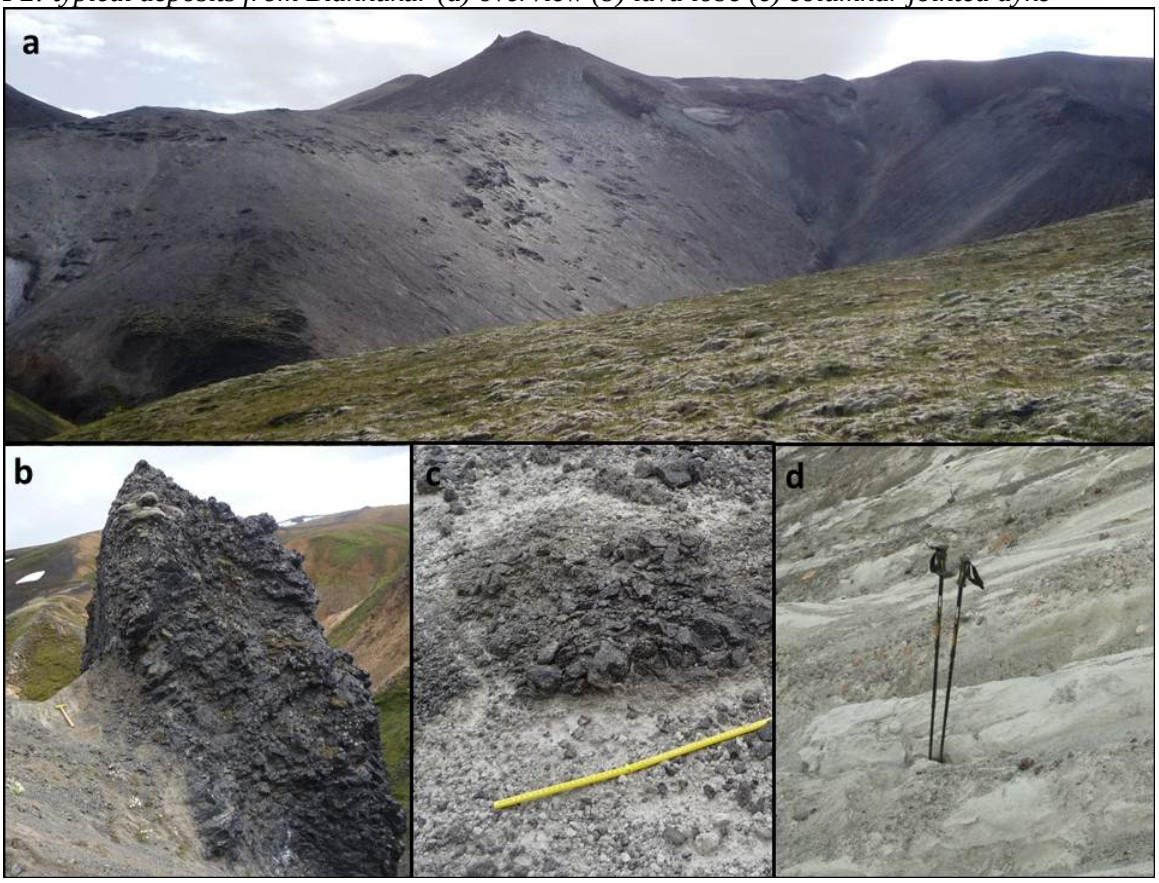

Figure DR3: typical deposits from Dalakvísl (a) overview (b) lava lobe (c) obsidian sheet (d) crudely bedded ash

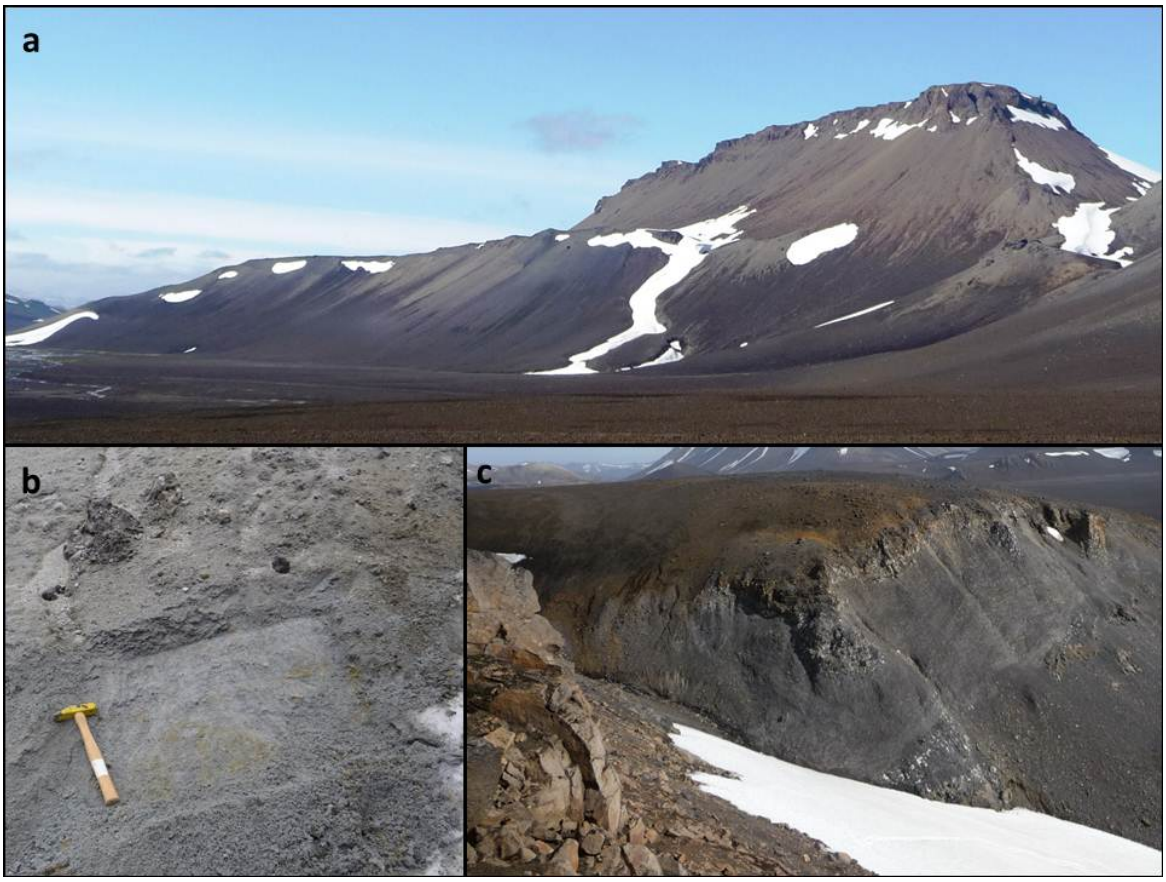

Figure DR4: typical deposits from SE Rauðfossafjöll (a) overview (b) fragmental deposit (c) lava cap (Eastern Plateau)

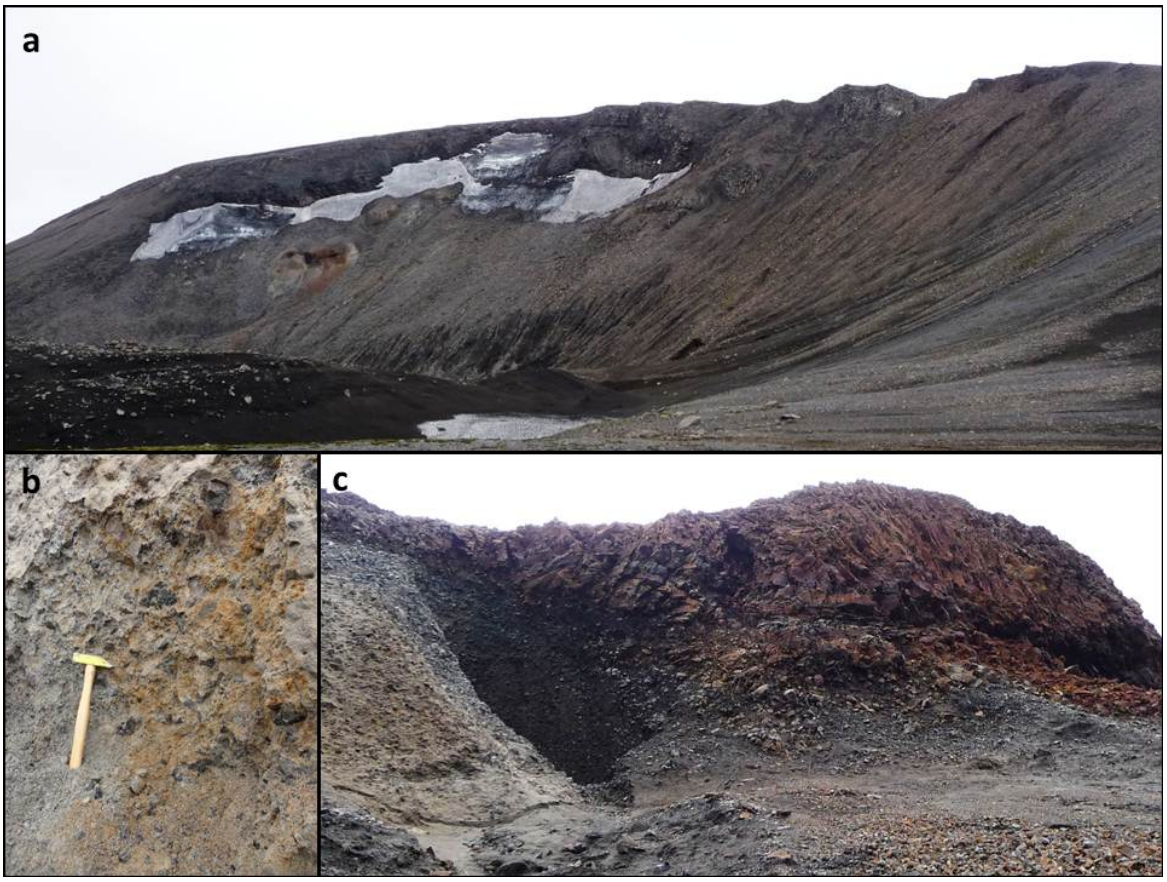

Figure DR5: typical deposits from NW Rauðfossafjöll (a) overview (b) fragmental deposit (c) subglacial to subaerial transition (fragmental deposit overlain by columnar jointed capping lava)

DR2. Grain size distributions

Sieving method

Fragmental deposits were collected from Bláhnúkur, Dalakvísl and SE Rauðfossafjöll. The samples were dried and then hand sieved with increasingly smaller aperture sizes stepping in one phi intervals. Each interval was weighed with a Precisa XT 320 mass balance readable to 1 mg.

Grain size results

Walker (1981) associated deposits with a high proportion (>80%) of fine material (< 1 mm) as Phreatoplinian. T3 shows the percentage of our fragmental samples with < 1mm grain size.

Table DR3: Percentage of grain size distribution < 1mm, for tephra samples collected from Bláhnúkur, Dalakvísl and SE Rauðfossafjöll

Bláhnúkur	**J9** 34%	**J5** 42%	**L10a** 64%		
Dalakvísl	**D2** 29%	**D16d** 52%	**D12c** 59%	**D7c** 87%	
SE Rauðfossafjöll	**R20** 27%	**R24e** 48%	**R24c** 55%	**R4b** 67%	**R30** 67%

Linking grain size and vesicularity to eruptive style

D7c collected from the crudely bedded ash deposit at Dalakvísl is the only sample with >80% <1mm (T3), suggestive of a very high level of explosivity (Walker, 1981). Variability within grain size distributions (T3) could reflect varying degrees of fragmentation and/or different modes of transportation and deposition (Stevenson et al., 2011). In addition to a fine grain size, explosive subglacial rhyolitic deposits are characterised by highly vesicular ash shards (Stevenson et al., 2011). SEM images of ash shards from Bláhnúkur, Dalakvísl and SE Rauðfossafjöll (Tuffen et al., 2002a; Tuffen et al., 2002b; Tuffen et al., 2008) show that that the most vesicle-rich deposits are found at Dalakvísl. We use the fine tephra (F3d, T3) and high vesicularity (F6) of Dalakvísl deposits to suggest that the most explosive activity of our sampled deposits was associated with the construction of this edifice.

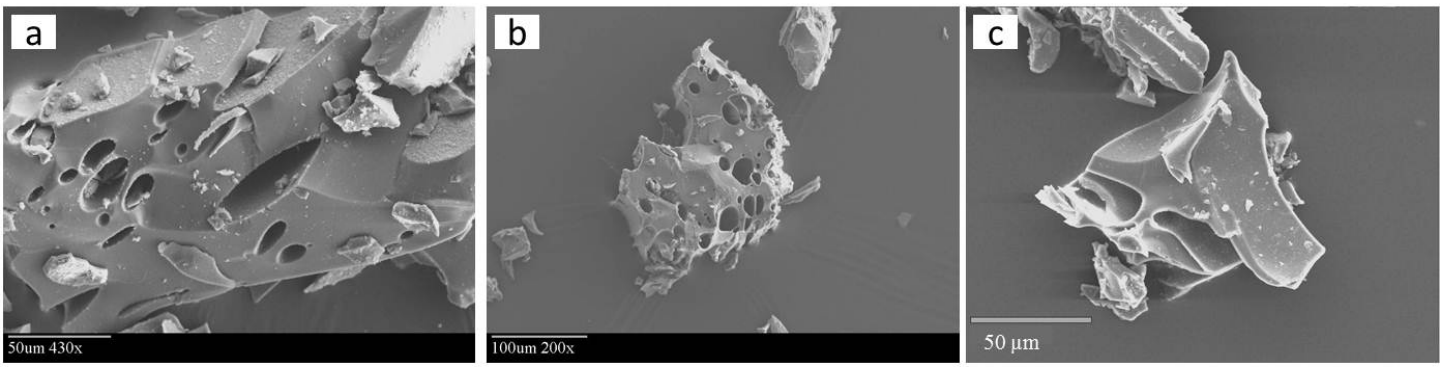

Figure DR6: SEM images of ash shards from (a) Bláhnúkur (Tuffen et al., 2002b) (b) Dalakvísl (Tuffen et al., 2008) and (c) SE Rauðfossafjöll (Tuffen et al., 2002a).

DR3. FTIR and identification of hydrated samples

Perlitic textures

In general we did not collect samples with perlitic textures (T1) (Denton et al., 2009). The exception, R20, was a variably perlitised clast, where we chose the most intact part for preparation of SIMS and FTIR wafers. FTIR and SIMS data both indicate matrix glass water contents of 0.12 wt.% (T4, T7) consistent with no post-quenching hydration.

There were no visible signs of perlitisation in any of the other samples, however, hydration can occur without leaving perlitic textures (Tuffen et al., 2010); thus a FTIR investigation was performed.

FTIR method

Fourier transform infrared spectroscopy (FTIR) was performed on every one of our samples that underwent SIMS investigation (T1). Thin slices of rock were cut and doubly polished to create wafers ~100-300 µm thick. Thicknesses were measured to within ± 3µm with a Mitutoyo digital displacement gauge and analyses conducted at the Open University, UK, using a Thermo Nicolet FTIR. To minimise background contamination, analyses were performed inside a N_2 purged tank and a background was taken for every sample. We used a Continuum Analytical microscope, KBr beamsplitter, MCT-A detector, and 100 µm square aperture. For every sample a minimum of five data points were collected within tens of µm of the spot where we measured the thickness. Measurements were run with 128 or 256 scans between 650 and 5000 cm^{-1} with a 4 cm^{-1} resolution. The spectra were analysed by applying a 15-point linear baseline correction.

Total water (H_2O_t) and molecular water (H_2O_m) contents (Ci) were measured using the 3550 and 1630 cm^{-1} peaks respectively and application of the Beer-Lambert Law

$$C_i = \frac{M_w Abs}{d\rho\varepsilon} \quad (1)$$

where M_w is the molecular weight of water (18.02 $gmol^{-1}$), Abs is absorbance level i.e. measured peak height, d is sample thickness (in cm) ρ is rock density (in gl^{-1}) and ε is absorption coefficient (in $lmol^{-1}$ cm^{-1}), i refers to the measured species; in our case H_2O_t and H_2O_m. We measured rock density using the Archimedes Principle on non-vesicular samples. Bláhnúkur samples were found to be 2.47 ± 0.03 g cm^{-3} (Owen et al., 2012) and Dalakvísl 2.41 ± 0.01 g cm^{-3} (Owen et al., unpublished data), which we have used for the Bláhnúkur and ring fracture densities respectively. Absorption coefficients of 80 $lmol^{-1}$ cm^{-1} (Leschik et al., 2004) and 55 $lmol^{-1}$ cm^{-1} (Newman et al., 1986) were used for the 3550 and 1630 cm^{-1} peaks respectively.

Cumulative errors for FTIR are commonly quoted as ±10% for H_2O_t and ±20% for H_2O_m (Owen et al., 2012).

FTIR results

Table DR4: FTIR data for all samples for which a SIMS analysis was performed, with the exceptions of R24a and D7b which produced oversaturated spectra.

Sample name	Analysis number	Density / gl^{-1}	thickness / cm	3550 cm^{-1} peak height	1630 cm^{-1} peak height	H_2O_t / wt.%	H_2O_m / wt.%
A1a	1	2414.714	0.0226	0.265	0.11	0.11	0.07
A1a	2	2414.714	0.0226	0.26	0.1	0.11	0.06
A1a	3	2414.714	0.0226	0.279	0.112	0.12	0.07
A1a	4	2414.714	0.0226	0.258	0.104	0.11	0.06
A1a	5	2414.714	0.0226	0.259	0.105	0.11	0.06
J2b	1_1	2472.501	0.0175	0.56	0.14	0.29	0.11
J2b	1_2	2472.501	0.0175	0.57	0.14	0.30	0.11
J2b	1_3	2472.501	0.0175	0.58	0.14	0.30	0.11
J2b	1_4	2472.501	0.0175	0.57	0.15	0.30	0.11
J2b	1_5	2472.501	0.0175	0.57	0.14	0.30	0.11
J2b	1_6	2472.501	0.0175	0.56	0.14	0.29	0.11
J2b	1_7	2472.501	0.0175	0.55	0.14	0.29	0.11
J2b	1_8	2472.501	0.0175	0.57	0.14	0.30	0.11
J2b	1_9	2472.501	0.0175	0.58	0.14	0.30	0.11
J2b	1_10	2472.501	0.0175	0.56	0.13	0.29	0.10
J2b	1_11	2472.501	0.0175	0.55	0.14	0.29	0.11
J2b	1_12	2472.501	0.0175	0.57	0.14	0.30	0.11
J2b	1_13	2472.501	0.0194	0.54	0.14	0.25	0.10
J2b	1_14	2472.501	0.0194	0.58	0.14	0.27	0.10
J2b	1_15	2472.501	0.0194	0.6	0.17	0.28	0.12
J2b	1_16	2472.501	0.0194	0.6	0.15	0.28	0.10
J2b	1_17	2472.501	0.0194	0.58	0.14	0.27	0.10
J2b	1_18	2472.501	0.0194	0.57	0.15	0.27	0.10
J2b	1_19	2472.501	0.0194	0.6	0.16	0.28	0.11
J2b	2_1	2472.501	0.0255	0.995	0.173	0.36	0.09
J2b	2_2	2472.501	0.0255	0.929	0.182	0.33	0.09
J2b	2_3	2472.501	0.0255	0.917	0.176	0.33	0.09
J2b	2_4	2472.501	0.0255	0.986	0.178	0.35	0.09
J2b	2_5	2472.501	0.0255	0.945	0.178	0.34	0.09
J3	1	2472.501	0.0177	1.18	0.26	0.61	0.19
J3	2	2472.501	0.0177	1.19	0.26	0.61	0.19
J3	3	2472.501	0.0177	1.14	0.25	0.59	0.19
J3	4	2472.501	0.0177	1.13	0.26	0.58	0.19
J3	5	2472.501	0.0177	1.17	0.26	0.60	0.19
J11	1	2472.501	0.0119	0.36	0.11	0.28	0.12
J11	2	2472.501	0.0119	0.33	0.13	0.25	0.14
J11	3	2472.501	0.0119	0.33	0.1	0.25	0.11
J11	4	2472.501	0.0119	0.34	0.1	0.26	0.11

J11	5	2472.501	0.0119	0.35	0.11	0.27	0.12
J11	6	2472.501	0.0119	0.35	0.13	0.27	0.14
J11	7	2472.501	0.0119	0.35	0.1	0.27	0.11
J11	8	2472.501	0.0119	0.35	0.1	0.27	0.11
J11	9	2472.501	0.0119	0.39	0.11	0.30	0.12
L8bott	1	2472.501	0.0129	1.24	0.34	0.88	0.35
L8bott	2	2472.501	0.0129	1.22	0.36	0.86	0.37
L8bott	3	2472.501	0.0129	1.22	0.36	0.86	0.37
L8bott	4	2472.501	0.0129	1.14	0.36	0.81	0.37
L8bott	5	2472.501	0.0169	1.12	0.28	0.60	0.22
L8bott	6	2472.501	0.0169	1.13	0.29	0.61	0.23
L8bott	7	2472.501	0.0169	1.16	0.29	0.63	0.23
L8bott	8	2472.501	0.0169	1.17	0.29	0.63	0.23
L8bott	9	2472.501	0.0163	1.03	0.21	0.58	0.17
L8bott	10	2472.501	0.0163	0.98	0.24	0.55	0.20
L8bott	11	2472.501	0.0163	1.03	0.24	0.58	0.20
L8bott	12	2472.501	0.0163	1.09	0.24	0.61	0.20
L8bott	13	2472.501	0.0163	1.06	0.23	0.59	0.19
L8bott	14	2472.501	0.0163	1.02	0.22	0.57	0.18
L8bott	15	2472.501	0.0163	1.03	0.23	0.58	0.19
D1	1	2414.714	0.0312	2.175	0.598	0.65	0.26
D1	2	2414.714	0.0312	1.953	0.57	0.58	0.25
D1	3	2414.714	0.0312	2.151	0.642	0.64	0.28
D1	4	2414.714	0.0312	2.22	0.625	0.66	0.27
D1	5	2414.714	0.0312	2.205	0.647	0.66	0.28
D13a	1	2414.714	0.0348	2.424	0.463	0.65	0.18
D13a	2	2414.714	0.0348	2.397	0.463	0.64	0.18
D13a	3	2414.714	0.0348	2.334	0.445	0.63	0.17
D13a	4	2414.714	0.0348	2.334	0.445	0.63	0.17
D13a	5	2414.714	0.0348	2.388	0.445	0.64	0.17
D22	1	2414.714	0.0204	1.159	0.256	0.53	0.17
D22	2	2414.714	0.0204	1.086	0.238	0.50	0.16
D22	3	2414.714	0.0204	1.078	0.247	0.49	0.16
D22	4	2414.714	0.0204	1.31	0.418	0.60	0.28
D22	5	2414.714	0.0204	1.216	0.272	0.56	0.18
R7bg	1	2414.714	0.017	0.165	0.131	0.09	0.10
R7bg	2	2414.714	0.017	0.197	0.139	0.11	0.11
R7bg	3	2414.714	0.017	0.197	0.111	0.11	0.09
R7bg	4	2414.714	0.017	0.214	0.134	0.12	0.11
R7bg	5	2414.714	0.017	0.235	0.161	0.13	0.13
R7bg	6	2414.714	0.017	0.153	0.125	0.08	0.10
R7hf	7	2414.714	0.0161	0.166	0.103	0.10	0.09
R7hf	8	2414.714	0.0161	0.165	0.106	0.10	0.09
R7hf	9	2414.714	0.0185	0.211	0.125	0.11	0.09

R7hf	10	2414.714	0.0185	0.206	0.122	0.10	0.09
R7hf	11	2414.714	0.0188	0.234	0.125	0.12	0.09
R7hf	12	2414.714	0.0188	0.224	0.123	0.11	0.09
R7hf	13	2414.714	0.0186	0.196	0.132	0.10	0.10
R7hf	14	2414.714	0.0186	0.194	0.131	0.10	0.10
R7hf	15	2414.714	0.0177	0.18	0.11	0.09	0.08
R7hf	16	2414.714	0.0177	0.175	0.128	0.09	0.10
R7hf	17	2414.714	0.0158	0.187	0.128	0.11	0.11
R7hf	18	2414.714	0.0158	0.166	0.125	0.10	0.11
R13	1	2414.714	0.0264	0.286	0.192	0.10	0.10
R13	2	2414.714	0.0264	0.288	0.203	0.10	0.10
R13	3	2414.714	0.0264	0.262	0.201	0.09	0.10
R13	4	2414.714	0.0264	0.283	0.216	0.10	0.11
R13	5	2414.714	0.0264	0.273	0.208	0.10	0.11
R20_ob	1	2414.71	0.0243	0.268	0.133	0.10	0.07
R20_ob	2	2414.71	0.0243	0.323	0.14	0.12	0.08
R20_ob	3	2414.71	0.0243	0.307	0.136	0.12	0.08
R20_ob	4	2414.71	0.0243	0.289	0.145	0.11	0.08
R20_ob	5	2414.71	0.0243	0.306	0.139	0.12	0.08
S1e	1	2414.71	0.0194	0.305	0.153	0.15	0.11
S1e	2	2414.71	0.0194	0.297	0.153	0.14	0.11
S1e	3	2414.71	0.0194	0.264	0.166	0.13	0.12
S1e	4	2414.71	0.0194	0.274	0.141	0.13	0.10
S1e	5	2414.71	0.0194	0.285	0.139	0.14	0.10

Water speciation

Since meteoric water is often added in the molecular form, FTIR provides a way of identifying hydrated samples by those having higher than expected ratios of molecular water (H_2O_m) to total water (H_2O_t) (Denton et al., 2009; Tuffen et al., 2010). The expected H_2O_m –H_2O_t relationships for non-hydrated and hydrated rhyolites have been well characterised (Owen et al., 2012). Since all of the samples in this study, and those in the (Owen et al., 2012; unpublished) papers, were collected from Torfajökull, erupted with similar compositions and temperatures and have been analysed using the same absorption coefficients, a direct comparison of water speciation is possible and this is plotted in F7. In F7 it can clearly be seen that our samples chosen for SIMS analysis (red stars) plot on the non-hydrated trend. Thus, we can be confident that these samples have not experienced hydration.

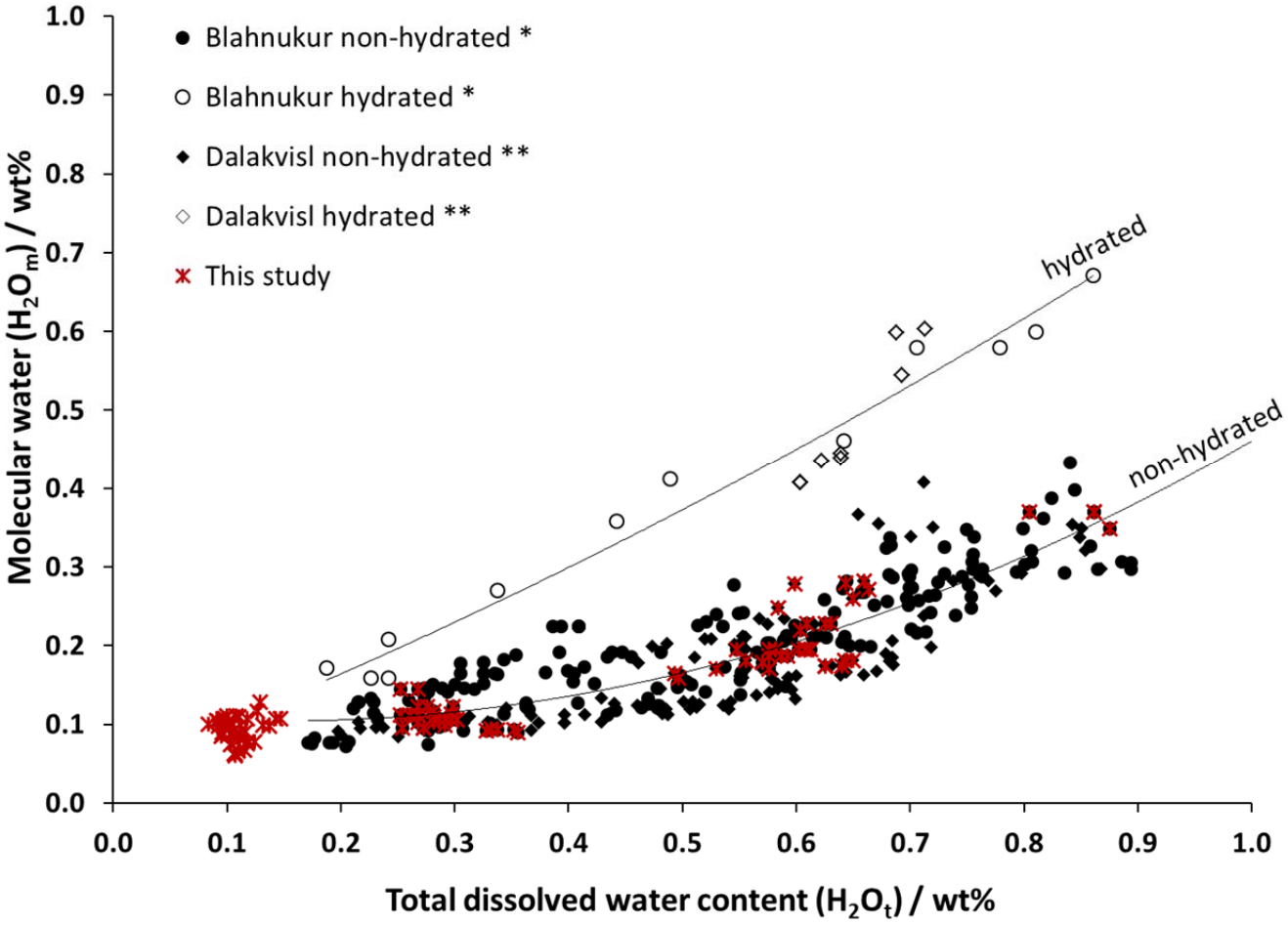

*Figure DR7: A speciation graph showing how data from this study (red stars) compares to data from Bláhnúkur (circles) and Dalakvísl (diamonds). Filled in and open shapes depict samples thought to be non-hydrated and hydrated, respectively. Polynomial trendlines (lines) have been fitted to these trends. * is data from Owen et al. (2012) and ** is data from Owen et al., (unpublished).*

Identifying hydrated samples

Despite not getting speciation data for R24a and D7b due to the FTIR spectra being oversaturated, we believe these samples to be hydrated. SIMS data reveals that R24a and D7b(1) contain >5 wt.% H_2O (T7) which is considerably more than the normal range for obsidian (< ~3 wt.%; Denton et al. (2009)) but is similar to the measured water content of Torfajökull perlites (Denton et al., 2009; Denton et al., 2012). We have therefore removed R24a and D7b(1) from our database.

For the remaining samples, FTIR analysis did prove successful and speciation data shows that all of these samples (T3) fit on trends consistent with the samples not being hydrated (F7). Thus, with samples R24a and D7b(1) removed, we are confident that the dataset does not include any water values modified by post-quenching hydration.

DR4. EPMA and determination of post-entrapment crystallisation

EPMA method

We analysed eight samples from Bláhnúkur and four samples from Dalakvísl (T1) for the major element chemistry of their matrix glass and MI. Where possible, we tried to perform SIMS and EPMA within the same MI, however, the MI were seldom large enough to allow for multiple analysis and repeated analysis on the same point should not be undertaken due to glass damage leading to erroneous results (Humphreys et al., 2006). Therefore, EPMA does not provide a direct reference for whether the MI investigated with SIMS have experienced post-entrapment crystallisation, but rather an indication for the likely trends of the Bláhnúkur and ring fracture eruptions.

Major element concentrations were determined by electron probe microanalysis (EPMA) at the University of Cambridge, UK. We used a Cameca SX-100 microprobe with an accelerating voltage of 15 keV, beam current of 4 nA and spot size of 10 µm. Standards were analysed daily.

Relative standard deviations for Si, Na and K were less than 1.5, 0.5 and 0.4 wt.% respectively.

EPMA results

Table DR5: Major element EPMA data from Bláhnúkur matrix glasses, melt inclusions and phenocrysts

Sample name	Material	Analysis number	Na_2O	MgO	SiO_2	K_2O	CaO	TiO_2	FeO	Al_2O_3	F	Cl	SO_2	P_2O_5	MnO	Total	Na_2O+K_2O
Matrix glass																	
J2b	MG	2_1	5.5	0.2	73.2	5.1	0.6	0.2	2.5	14.2	0.3	0.2	0.0	0.0	0.1	102.2	10.6
J2b	MG	2_2	5.5	0.1	72.5	5.3	0.6	0.2	2.6	14.2	0.3	0.2	0.0	0.0	0.0	101.6	10.8
J2b	MG	2_3	5.6	0.1	73.0	5.2	0.7	0.2	2.5	14.4	0.3	0.2	0.0	0.0	0.1	102.2	10.8
J2b	MG	2_4	5.5	0.2	72.9	5.2	0.6	0.2	2.4	14.0	0.4	0.2	0.0	0.0	0.1	101.7	10.7
J2b	MG	2_5	5.6	0.1	73.0	5.4	0.6	0.2	2.6	14.2	0.4	0.2	0.0	0.0	0.1	102.3	10.9
J2b	MG	2_6	6.1	0.1	74.1	4.1	0.7	0.2	2.6	13.8	0.2	0.2	0.0	0.0	0.1	102.1	10.2
J2b	MG	2_7	6.3	0.0	74.2	4.0	0.4	0.2	1.9	14.0	0.2	0.2	0.0	0.0	0.1	101.6	10.4
J2b	MG	2_8	5.8	0.0	73.9	4.8	0.3	0.2	2.3	14.0	0.3	0.2	0.0	0.0	0.0	101.9	10.5
J2b	MG	2_9	6.0	0.1	73.7	4.3	0.5	0.2	2.2	13.9	0.2	0.2	0.0	0.0	0.0	101.3	10.4
J2b	MG	2_10	6.2	0.2	73.0	3.9	1.1	0.2	2.9	14.1	0.1	0.1	0.0	0.0	0.1	102.0	10.1
J2b	MG	2_11	5.7	0.1	72.6	5.1	0.4	0.2	2.5	13.9	0.3	0.2	0.0	0.0	0.1	101.2	10.9
J2b	MG	2_12	5.5	0.1	72.8	5.3	0.4	0.2	2.7	14.1	0.3	0.2	0.0	0.0	0.1	101.6	10.8
J2b	MG	2_13	5.6	0.1	73.3	5.3	0.4	0.2	2.4	14.2	0.3	0.2	0.0	0.0	0.0	102.0	10.9
J2b	MG	2_14	5.7	0.0	73.8	4.9	0.4	0.2	2.2	13.8	0.3	0.2	0.0	0.0	0.1	101.5	10.6
J2b	MG	2_15	5.5	0.1	73.1	5.2	0.4	0.2	2.2	14.1	0.3	0.2	0.0	0.0	0.1	101.4	10.7
J2b	MG	2_16	5.6	0.0	73.3	5.1	0.3	0.2	2.3	14.3	0.3	0.2	0.0	0.0	0.1	101.6	10.7
J2b	MG	2_17	5.7	0.0	73.3	5.3	0.3	0.2	2.2	14.2	0.3	0.2	0.0	0.0	0.1	101.8	11.0
J2b	MG	2_18	6.5	0.0	73.0	4.3	0.5	0.2	1.9	14.6	0.2	0.1	0.0	0.0	0.1	101.5	10.7
J2b	MG	2_19	5.8	0.0	73.3	5.1	0.3	0.2	2.2	14.5	0.3	0.2	0.0	0.0	0.1	102.0	10.9
J2b	MG	2_20	5.7	0.1	73.4	5.3	0.3	0.2	2.1	14.2	0.3	0.2	0.0	0.0	0.0	101.9	11.0
J2b	MG	2_21	6.0	0.1	72.9	4.3	1.0	0.2	2.8	14.1	0.2	0.1	0.0	0.0	0.1	101.9	10.3
J2b	MG	2_22	5.6	0.1	72.6	4.9	0.9	0.2	2.7	14.0	0.2	0.2	0.0	0.0	0.1	101.6	10.6
J2b	MG	2_23	5.6	0.2	72.3	5.1	0.7	0.2	2.9	14.1	0.3	0.2	0.0	0.0	0.1	101.6	10.6

J2b	MG	2_24	5.5	0.2	72.9	5.3	0.7	0.2	2.9	13.8	0.3	0.2	0.0	0.0	0.1	102.0	10.8
J2b	MG	2_25	5.9	0.1	73.0	4.5	0.9	0.2	2.7	14.3	0.2	0.1	0.0	0.0	0.1	102.1	10.4
J2b	MG	2_26	5.7	0.0	73.3	5.1	0.3	0.2	2.3	14.3	0.2	0.2	0.0	0.0	0.0	101.9	10.8
J2b	MG	2_27	5.5	0.1	72.7	5.1	0.5	0.2	2.3	14.0	0.3	0.2	0.0	0.0	0.1	100.9	10.7
J2b	MG	2_29	5.6	0.1	72.5	5.0	0.6	0.3	2.3	14.0	0.3	0.2	0.0	0.0	0.1	101.0	10.7
J2b	MG	2_30	5.8	0.1	73.4	5.1	0.5	0.2	2.5	14.3	0.2	0.2	0.0	0.0	0.1	102.5	10.9
J2b	MG	2_31	5.6	0.1	72.2	5.1	0.6	0.2	2.4	14.0	0.3	0.2	0.0	0.0	0.1	100.8	10.7
J2b	MG	2_32	5.5	0.1	72.9	5.2	0.6	0.2	2.4	14.1	0.3	0.2	0.0	0.0	0.1	101.5	10.8
J2b	MG	2_33	5.6	0.1	72.4	5.2	0.6	0.2	2.6	14.0	0.3	0.2	0.0	0.0	0.1	101.4	10.8
J2b	MG	2_34	5.6	0.1	72.8	5.3	0.6	0.2	2.4	14.0	0.3	0.2	0.0	0.0	0.1	101.4	10.9
J2b	MG	2_35	5.5	0.1	72.9	5.4	0.6	0.2	2.4	14.0	0.3	0.2	0.0	0.0	0.1	101.6	10.9
J2b	MG	2_36	5.5	0.1	72.5	5.4	0.6	0.2	2.5	13.8	0.3	0.2	0.0	0.0	0.1	101.1	10.8
J2b	MG	2_37	5.2	0.1	73.2	5.5	0.5	0.1	2.4	14.2	0.3	0.2	0.0	0.0	0.1	101.9	10.8
J2b	MG	2_38	5.3	0.1	72.8	5.4	0.5	0.2	2.3	13.9	0.3	0.2	0.0	0.0	0.1	101.1	10.7
J2b	MG	2_39	5.4	0.1	73.0	5.2	0.6	0.2	2.6	14.1	0.3	0.2	0.0	0.0	0.1	101.8	10.6
J2b	MG	2_40	5.6	0.1	72.6	5.1	0.6	0.2	2.4	14.2	0.3	0.2	0.0	0.0	0.1	101.4	10.7
J2b	MG	2_41	5.6	0.1	72.2	5.3	0.5	0.2	2.4	14.1	0.3	0.2	0.0	0.0	0.1	100.9	10.9
J2b	MG	2_42	5.4	0.1	72.4	5.3	0.6	0.2	2.4	14.2	0.3	0.2	0.0	0.0	0.1	101.2	10.7
J2b	MG	2_43	5.7	0.1	73.6	4.9	0.4	0.2	2.5	14.1	0.3	0.2	0.0	0.0	0.1	101.9	10.6
J2b	MG	2_44	6.0	0.1	72.9	4.7	0.5	0.2	2.4	14.2	0.3	0.2	0.0	0.0	0.1	101.4	10.7
J2b	MG	2_45	5.6	0.1	73.0	5.0	0.5	0.2	2.3	14.1	0.3	0.2	0.0	0.0	0.1	101.3	10.7
J2b	MG	2_46	5.6	0.1	73.3	5.1	0.5	0.2	2.5	14.1	0.3	0.2	0.0	0.0	0.1	101.9	10.7
J2b	MG	2_47	5.7	0.1	73.3	5.1	0.5	0.2	2.2	14.3	0.3	0.2	0.0	0.0	0.1	101.9	10.8
J2b	MG	2_48	5.5	0.1	72.8	5.4	0.6	0.2	2.6	14.2	0.3	0.2	0.0	0.0	0.1	101.9	10.9
J3	MG	2_1	5.7	0.1	72.7	4.8	0.6	0.2	2.5	14.1	0.3	0.2	0.0	0.0	0.1	101.3	10.5
J3	MG	2_2	5.6	0.1	72.8	4.9	0.6	0.2	2.3	14.1	0.2	0.2	0.0	0.0	0.1	101.3	10.6
J3	MG	2_3	5.7	0.1	72.4	4.9	0.6	0.2	2.5	14.3	0.2	0.2	0.0	0.0	0.0	101.2	10.6
J3	MG	2_4	5.7	0.1	72.6	5.0	0.6	0.2	2.4	14.3	0.3	0.2	0.0	0.0	0.1	101.4	10.8
J3	MG	2_5	5.6	0.1	72.3	4.8	0.6	0.2	2.4	14.2	0.2	0.2	0.0	0.0	0.1	100.7	10.4
J3	MG	2_6	6.9	0.0	73.6	3.7	0.6	0.2	1.7	15.0	0.1	0.1	0.0	0.0	0.0	102.1	10.6
J3	MG	2_7	5.9	0.1	72.2	4.8	0.4	0.2	2.2	14.1	0.3	0.2	0.0	0.0	0.1	100.5	10.7
J3	MG	2_8	5.6	0.1	72.0	5.2	0.5	0.2	2.2	14.2	0.3	0.2	0.0	0.0	0.1	100.6	10.8
J3	MG	2_9	5.7	0.1	72.9	5.0	0.5	0.2	2.0	14.3	0.3	0.2	0.0	0.0	0.1	101.1	10.6
J3	MG	2_10	5.6	0.1	72.5	5.3	0.4	0.2	2.1	14.0	0.3	0.2	0.0	0.0	0.1	100.7	10.8
J5	MG	1_5	5.7	0.1	72.8	4.9	0.4	0.2	1.9	13.9	0.2	0.2	0.0	0.0	0.0	100.4	10.7
J5	MG	2_4	6.1	0.1	73.1	4.8	0.5	0.2	2.6	13.7	0.3	0.3	0.0	0.0	0.1	101.7	10.8
J5	MG	2_5	5.2	0.0	72.5	5.8	0.4	0.2	2.4	13.9	0.5	0.2	0.0	0.0	0.1	101.4	11.0
J5	MG	2_6	5.9	0.1	73.8	4.5	0.5	0.2	2.2	14.2	0.2	0.1	0.0	0.0	0.1	101.8	10.5
J5	MG	2_8	5.3	0.1	72.7	5.5	0.5	0.2	2.3	14.2	0.3	0.2	0.0	0.0	0.1	101.4	10.7
J5	MG	2_9	5.3	0.1	73.0	5.5	0.4	0.2	2.4	14.1	0.3	0.2	0.0	0.0	0.0	101.7	10.9
J5	MG	2_10	5.2	0.1	72.9	5.6	0.5	0.2	2.4	14.2	0.3	0.2	0.0	0.0	0.1	101.7	10.8
J5	MG	3_4	5.3	0.1	72.8	5.7	0.4	0.2	2.2	14.2	0.3	0.2	0.0	0.0	0.1	101.4	11.0
J5	MG	3_5	5.3	0.1	73.7	5.2	0.4	0.2	2.0	13.8	0.3	0.2	0.0	0.0	0.1	101.3	10.4
J5	MG	3_6	5.1	0.1	73.1	5.7	0.4	0.2	2.3	14.1	0.3	0.2	0.0	0.0	0.1	101.5	10.7

J5	MG	3_7	5.7	0.0	72.6	5.0	0.4	0.2	2.1	14.0	0.3	0.2	0.0	0.0	0.1	100.8	10.7
J5	MG	3_8	5.3	0.1	73.0	5.6	0.4	0.2	2.1	14.0	0.3	0.2	0.0	0.0	0.1	101.3	10.9
J5	MG	3_9	5.2	0.1	73.1	5.6	0.4	0.2	2.4	14.1	0.4	0.2	0.0	0.0	0.1	101.7	10.8
J5	MG	3_10	5.6	0.1	72.6	5.2	0.4	0.2	2.7	14.2	0.3	0.2	0.0	0.0	0.1	101.6	10.8
J5	MG	3_11	5.3	0.1	72.5	5.5	0.4	0.2	2.1	13.8	0.3	0.2	0.0	0.0	0.0	100.5	10.8
J5	MG	3_12	5.2	0.1	72.6	5.6	0.4	0.2	2.0	14.2	0.4	0.2	0.0	0.0	0.1	101.1	10.8
J10	*MG*	*2_1*	*7.4*	*0.1*	*70.2*	*4.5*	*0.8*	*0.1*	*1.7*	*17.2*	*0.2*	*0.1*	*0.0*	*0.0*	*0.0*	*102.4*	*11.9*
J10	MG	2_2	4.9	0.1	75.8	5.2	0.4	0.3	2.5	12.1	0.3	0.3	0.0	0.0	0.1	102.1	10.1
J10	MG	2_3	4.9	0.1	74.7	5.2	0.5	0.2	2.8	12.4	0.4	0.3	0.0	0.0	0.1	101.7	10.1
J10	MG	2_4	5.6	0.1	73.4	5.0	0.5	0.2	2.1	13.8	0.3	0.2	0.0	0.0	0.1	101.3	10.6
J10	*MG*	*2_5*	*6.8*	*0.1*	*72.2*	*4.6*	*0.6*	*0.2*	*1.7*	*16.2*	*0.2*	*0.1*	*0.0*	*0.0*	*0.0*	*102.8*	*11.5*
J10	*MG*	*3_4*	*6.1*	*0.1*	*73.3*	*4.8*	*0.6*	*0.2*	*2.1*	*14.9*	*0.2*	*0.2*	*0.0*	*0.0*	*0.0*	*102.5*	*11.0*
J10	*MG*	*3_5*	*8.4*	*0.2*	*68.0*	*3.8*	*1.3*	*0.0*	*0.9*	*18.9*	*0.0*	*0.0*	*0.0*	*0.0*	*0.1*	*101.7*	*12.2*
J10	*MG*	*3_6*	*8.1*	*0.0*	*68.0*	*5.2*	*0.8*	*0.0*	*0.5*	*19.4*	*0.0*	*0.0*	*0.0*	*0.0*	*0.0*	*102.0*	*13.3*
J11	MG	1_4	5.1	0.0	75.2	5.3	0.4	0.2	2.2	12.9	0.4	0.2	0.0	0.0	0.1	102.1	10.4
J11	MG	1_5	6.4	0.0	73.5	5.2	0.4	0.1	1.7	14.8	0.3	0.1	0.0	0.0	0.1	102.7	11.6
J11	*MG*	*1_6*	*6.9*	*0.0*	*71.8*	*5.1*	*0.5*	*0.1*	*1.5*	*16.5*	*0.1*	*0.1*	*0.0*	*0.0*	*0.0*	*102.7*	*11.9*
J11	MG	1_7	5.8	0.0	73.1	5.2	0.4	0.1	1.9	14.5	0.4	0.2	0.0	0.0	0.1	101.7	11.0
J11	*MG*	*1_8*	*7.0*	*0.0*	*72.2*	*5.0*	*0.5*	*0.1*	*1.2*	*16.3*	*0.2*	*0.1*	*0.0*	*0.0*	*0.1*	*102.6*	*12.0*
J11	*MG*	*2_4*	*6.8*	*0.0*	*72.9*	*4.9*	*0.6*	*0.1*	*1.2*	*16.0*	*0.2*	*0.1*	*0.0*	*0.0*	*0.0*	*102.9*	*11.7*
J11	MG	2_5	5.4	0.1	74.8	5.1	0.4	0.2	2.0	13.2	0.3	0.2	0.0	0.0	0.1	101.7	10.4
J11	*MG*	*2_6*	*8.4*	*0.0*	*69.0*	*4.5*	*0.7*	*0.0*	*0.5*	*19.2*	*0.0*	*0.0*	*0.0*	*0.0*	*0.0*	*102.4*	*12.9*
L6c	MG	2_1	5.3	0.1	72.9	5.0	0.5	0.2	2.3	14.1	0.3	0.2	0.0	0.0	0.1	101.1	10.4
L6c	MG	2_2	5.5	0.1	72.5	5.3	0.5	0.2	2.2	13.9	0.3	0.2	0.0	0.0	0.1	100.8	10.8
L6c	MG	2_3	5.7	0.0	72.3	5.2	0.4	0.2	1.7	13.8	0.3	0.2	0.0	0.0	0.1	99.9	10.8
L6c	MG	2_4	5.4	0.1	72.6	5.2	0.5	0.2	2.1	13.7	0.3	0.2	0.0	0.0	0.1	100.4	10.6
L6c	MG	2_5	5.5	0.1	71.9	5.2	0.5	0.2	2.2	13.9	0.3	0.2	0.0	0.0	0.1	100.0	10.6
L6c	MG	2_6	5.5	0.1	72.4	5.0	0.4	0.1	2.2	13.9	0.3	0.2	0.0	0.0	0.1	100.1	10.4
L6c	MG	2_7	5.4	0.1	71.9	5.0	0.5	0.2	2.4	13.6	0.3	0.2	0.0	0.0	0.1	99.6	10.3
L6c	MG	2_8	5.4	0.1	73.0	5.1	0.3	0.1	1.7	14.0	0.3	0.2	0.0	0.0	0.1	100.2	10.4
L6c	MG	2_9	5.3	0.0	71.3	5.1	0.5	0.2	2.3	13.9	0.3	0.2	0.0	0.0	0.1	99.3	10.5
L6c	MG	2_10	5.5	0.1	72.3	5.2	0.5	0.2	2.4	13.8	0.3	0.2	0.0	0.0	0.1	100.5	10.7
L8bott	MG	2_1	5.5	0.1	72.8	5.1	0.4	0.2	2.3	14.0	0.3	0.2	0.0	0.0	0.1	100.9	10.5
L8bott	MG	2_2	5.7	0.1	72.5	5.2	0.4	0.2	2.3	13.9	0.3	0.2	0.0	0.0	0.1	100.9	10.9
L8bott	MG	2_3	5.8	0.0	72.9	4.9	0.4	0.2	2.2	14.2	0.3	0.2	0.0	0.0	0.0	101.1	10.7
L8bott	MG	2_4	5.6	0.0	72.3	5.3	0.4	0.2	2.3	14.0	0.3	0.2	0.0	0.0	0.1	100.7	10.9
L8bott	MG	2_5	5.5	0.1	72.8	5.1	0.4	0.2	2.5	13.9	0.3	0.2	0.0	0.0	0.1	101.0	10.6
L8bott	MG	2_6	5.6	0.0	72.5	5.1	0.4	0.2	2.3	13.9	0.3	0.2	0.0	0.0	0.1	100.7	10.7
L8bott	MG	2_7	5.7	0.1	72.7	5.2	0.5	0.2	2.1	14.0	0.3	0.2	0.0	0.0	0.1	101.0	10.8
L8bott	MG	2_8	5.6	0.1	72.0	5.2	0.4	0.2	2.6	13.9	0.3	0.2	0.0	0.0	0.1	100.6	10.8
L8bott	MG	2_9	6.0	0.1	73.2	4.5	0.4	0.3	2.1	14.0	0.2	0.2	0.0	0.0	0.1	101.1	10.5
L8bott	MG	2_10	5.4	0.1	72.6	5.3	0.4	0.2	2.4	14.1	0.3	0.2	0.0	0.0	0.1	101.2	10.8
L8bott	MG	2_11	5.6	0.1	72.6	5.0	0.5	0.2	2.1	13.9	0.3	0.2	0.0	0.0	0.1	100.5	10.6
L8bott	MG	2_12	5.6	0.1	73.0	5.0	0.5	0.2	2.3	14.0	0.3	0.2	0.0	0.0	0.1	101.3	10.6

L8bott	MG	2_13	5.7	0.1	73.1	4.9	0.4	0.2	2.1	14.0	0.3	0.2	0.0	0.0	0.1	101.1	10.6
L8bott	MG	2_14	5.6	0.1	72.9	5.0	0.5	0.2	2.2	14.0	0.3	0.2	0.0	0.0	0.1	101.0	10.6
L8bott	MG	2_15	5.6	0.1	72.9	5.1	0.5	0.2	2.5	14.2	0.3	0.2	0.0	0.0	0.1	101.6	10.7
L8bott	MG	2_16	5.6	0.1	72.6	5.0	0.4	0.2	2.0	14.1	0.3	0.2	0.0	0.0	0.1	100.8	10.7
L8bott	MG	2_17	5.6	0.1	73.2	5.0	0.5	0.2	2.8	14.1	0.3	0.2	0.0	0.0	0.1	101.9	10.5
L8bott	MG	2_18	5.6	0.1	72.7	5.1	0.5	0.2	2.7	14.1	0.3	0.2	0.0	0.0	0.1	101.6	10.7
L8bott	MG	2_19	5.6	0.1	72.5	5.1	0.4	0.2	2.3	14.0	0.3	0.2	0.0	0.0	0.1	100.8	10.7
L8bott	MG	2_20	5.8	0.1	73.4	5.0	0.5	0.2	2.3	14.1	0.3	0.2	0.0	0.0	0.1	101.9	10.7
L8bott	MG	2_21	5.6	0.1	72.5	5.1	0.4	0.2	2.3	14.1	0.3	0.2	0.0	0.0	0.1	100.8	10.6
L8bott	MG	2_22	5.6	0.1	73.6	5.0	0.4	0.2	2.2	14.0	0.3	0.2	0.0	0.0	0.1	101.8	10.7
L8bott	MG	2_23	5.6	0.0	73.5	5.2	0.4	0.2	2.0	14.0	0.3	0.2	0.0	0.0	0.1	101.4	10.8
L8bott	MG	2_24	5.7	0.1	72.5	5.1	0.5	0.2	2.3	14.3	0.3	0.2	0.0	0.0	0.1	101.2	10.7
L8bott	MG	2_25	5.5	0.1	72.8	5.2	0.5	0.2	2.1	14.0	0.3	0.2	0.0	0.0	0.1	101.0	10.7
L8bott	MG	2_26	5.6	0.0	72.8	5.2	0.4	0.2	2.4	14.3	0.3	0.2	0.0	0.0	0.1	101.6	10.8
L8bott	MG	2_27	5.6	0.1	73.1	5.0	0.5	0.2	2.4	14.4	0.3	0.2	0.0	0.0	0.1	101.8	10.6
L8bott	MG	2_28	5.7	0.1	73.1	5.1	0.5	0.2	2.5	14.2	0.3	0.2	0.0	0.0	0.1	102.0	10.7
L8bott	MG	2_29	5.4	0.0	71.0	5.1	0.4	0.2	2.4	13.6	0.3	0.2	0.0	0.0	0.1	98.8	10.5
L8bott	MG	2_30	5.7	0.1	70.4	4.9	0.5	0.2	2.3	14.0	0.3	0.2	0.0	0.0	0.0	98.5	10.6
L8bott	MG	2_31	5.5	0.1	70.5	5.2	0.4	0.2	2.2	13.7	0.3	0.2	0.0	0.0	0.1	98.3	10.7
L8bott	MG	2_32	5.7	0.1	70.8	5.2	0.5	0.2	2.3	13.8	0.3	0.2	0.0	0.0	0.1	99.1	10.9
L8bott	MG	2_33	5.7	0.1	71.3	5.0	0.4	0.2	2.5	13.7	0.3	0.2	0.0	0.0	0.1	99.4	10.7
B2	MG	1_5	5.2	0.1	71.7	5.0	0.7	0.3	2.6	13.8	0.3	0.2	0.0	0.0	0.1	99.9	10.2
B2	MG	1_6	5.3	0.2	71.3	5.1	0.6	0.3	2.6	13.9	0.4	0.2	0.0	0.0	0.1	99.9	10.4
B2	MG	1_7	5.2	0.2	71.5	5.1	0.6	0.2	2.7	13.7	0.3	0.2	0.0	0.0	0.1	100.0	10.3
B2	MG	1_8	5.3	0.1	71.6	5.0	0.6	0.2	2.5	13.9	0.3	0.2	0.0	0.0	0.1	99.9	10.3
Melt inclusions																	
J2b	MI	1_1	7.9	0.1	73.6	2.3	0.6	0.2	2.5	14.3	0.2	0.2	0.0	0.0	0.1	101.9	10.2
J2b	MI	1_2	8.2	0.2	73.6	1.6	0.6	0.2	2.9	13.9	0.1	0.3	0.0	0.0	0.1	101.7	9.8
J2b	MI	1_3	5.3	0.1	72.3	5.6	0.5	0.2	3.0	13.9	0.4	0.3	0.0	0.0	0.1	101.7	10.9
J2b	MI	1_4	4.8	0.1	73.2	6.0	0.6	0.2	2.4	13.5	0.4	0.3	0.0	0.0	0.1	101.6	10.8
J2b	*MI*	*1_5*	*8.7*	*0.0*	*64.5*	*1.3*	*4.1*	*0.0*	*0.5*	*22.8*	*0.0*	*0.0*	*0.0*	*0.0*	*0.0*	*101.9*	*10.0*
J2b	*MI*	*1_6*	*8.2*	*0.0*	*62.8*	*0.8*	*5.9*	*0.0*	*0.3*	*24.2*	*0.0*	*0.0*	*0.0*	*0.0*	*0.0*	*102.3*	*9.0*
J3	MI	1_1	5.0	0.1	74.2	4.6	0.5	0.3	2.5	12.8	0.2	0.2	0.0	0.0	0.1	100.6	9.7
J3	MI	1_2	5.5	0.1	72.8	5.1	0.6	0.2	2.4	14.3	0.3	0.3	0.0	0.0	0.1	101.8	10.7
J3	MI	1_3	5.3	0.0	71.4	5.1	0.5	0.2	2.0	13.6	0.3	0.2	0.0	0.0	0.1	98.8	10.4
J5	*MI*	*2_1*	*8.9*	*0.1*	*68.3*	*2.8*	*1.0*	*0.0*	*1.0*	*18.5*	*0.0*	*0.1*	*0.0*	*0.0*	*0.0*	*100.7*	*11.7*
J5	*MI*	*2_2*	*9.3*	*0.0*	*68.7*	*3.1*	*1.2*	*0.0*	*0.3*	*20.2*	*0.0*	*0.0*	*0.0*	*0.0*	*0.0*	*102.8*	*12.4*
J5	MI	2_3	4.6	0.1	73.5	5.4	0.6	0.2	3.2	12.6	0.2	0.2	0.0	0.0	0.1	100.8	10.0
J5	MI	3_1	5.4	0.2	75.4	4.2	0.4	0.3	3.2	10.9	0.1	0.3	0.0	0.0	0.1	100.6	9.7
J5	MI	3_2	5.0	0.2	72.2	5.6	0.6	0.2	2.6	14.1	0.5	0.3	0.0	0.0	0.1	101.5	10.6
J5	*MI*	*3_3*	*9.4*	*0.0*	*68.8*	*3.2*	*0.6*	*0.0*	*0.7*	*19.5*	*0.0*	*0.0*	*0.0*	*0.0*	*0.0*	*102.3*	*12.6*
J10	MI	1_1	5.0	0.2	73.0	5.6	0.5	0.3	3.0	13.2	0.5	0.3	0.0	0.0	0.1	101.6	10.5
J10	MI	1_2	4.7	0.1	74.1	5.4	0.5	0.2	3.7	12.0	0.4	0.3	0.0	0.0	0.1	101.7	10.2
J10	MI	1_3	4.3	0.1	75.5	5.3	0.4	0.3	3.1	11.6	0.4	0.3	0.0	0.0	0.1	101.5	9.6

J10	MI	3_1	4.4	0.2	74.8	5.4	0.4	0.3	3.1	11.7	0.4	0.3	0.0	0.0	0.1	101.1	9.8
J10	MI	3_2	4.4	0.1	75.2	5.4	0.4	0.3	3.4	11.6	0.4	0.3	0.0	0.0	0.1	101.8	9.8
J10	*MI*	*3_3*	*7.8*	*0.1*	*70.3*	*4.3*	*0.7*	*0.0*	*1.1*	*17.5*	*0.1*	*0.1*	*0.0*	*0.0*	*0.0*	*101.9*	*12.1*
J11	MI	1_1	4.8	0.1	73.7	5.3	0.6	0.2	2.9	11.6	0.3	0.3	0.0	0.0	0.1	100.1	10.1
J11	MI	1_2	5.1	0.2	74.8	5.0	0.4	0.3	3.2	11.7	0.3	0.2	0.0	0.0	0.1	101.3	10.1
J11	MI	1_3	4.1	0.1	75.8	5.1	0.4	0.3	3.5	10.8	0.5	0.4	0.0	0.0	0.2	101.2	9.2
J11	MI	2_1	4.3	0.1	75.1	5.4	0.4	0.2	3.1	11.8	0.5	0.3	0.0	0.0	0.1	101.5	9.8
J11	MI	2_2	4.2	0.1	76.3	5.4	0.5	0.3	3.2	10.9	0.5	0.3	0.0	0.0	0.1	101.9	9.6
J11	MI	2_3	4.1	0.2	75.2	5.1	0.4	0.3	3.8	11.0	0.5	0.4	0.0	0.0	0.1	101.0	9.2
L6c	MI	1_1	5.0	0.1	73.5	5.3	0.5	0.2	2.9	12.1	0.4	0.4	0.0	0.0	0.1	100.5	10.3
L6c	*MI*	*1_2*	*9.2*	*0.1*	*67.4*	*2.5*	*1.8*	*0.0*	*0.4*	*20.8*	*0.0*	*0.0*	*0.0*	*0.0*	*0.0*	*102.1*	*11.7*
L6c	MI	1_3	4.9	0.1	74.1	5.1	0.5	0.2	2.9	12.7	0.4	0.4	0.0	0.0	0.1	101.5	10.0
L6c	MI	2_11	5.0	0.2	73.8	4.9	0.5	0.3	2.9	12.3	0.3	0.3	0.0	0.0	0.1	100.6	9.9
L6c	*MI*	*2_12*	*9.1*	*0.0*	*66.4*	*2.6*	*1.8*	*0.0*	*0.3*	*20.9*	*0.0*	*0.0*	*0.0*	*0.0*	*0.0*	*101.3*	*11.7*
L6c	MI	2_13	4.6	0.1	76.2	4.7	0.5	0.4	3.3	10.8	0.3	0.3	0.0	0.0	0.1	101.2	9.2
L6c	*MI*	*2_14*	*9.4*	*0.0*	*67.5*	*2.7*	*1.7*	*0.0*	*0.4*	*20.8*	*0.0*	*0.0*	*0.0*	*0.0*	*0.0*	*102.6*	*12.1*
L6c	MI	2_15	4.8	0.1	74.3	4.9	0.5	0.3	3.2	10.2	0.3	0.3	0.0	0.0	0.1	99.1	9.6
L8bott	MI	1_1	5.6	0.2	72.9	5.0	0.6	0.2	2.9	13.3	0.4	0.3	0.0	0.0	0.1	101.4	10.6
L8bott	MI	1_2	5.6	0.0	73.1	5.1	0.6	0.2	2.5	13.8	0.4	0.3	0.0	0.0	0.1	101.6	10.7
L8bott	MI	1_3	5.4	0.1	73.0	5.0	0.5	0.2	2.9	13.7	0.3	0.3	0.0	0.0	0.1	101.6	10.4
B2	MI	1_1	7.1	0.1	70.3	3.6	0.9	0.1	1.3	16.2	0.1	0.1	0.0	0.0	0.0	100.0	10.8
B2	*MI*	*1_2*	*8.3*	*0.0*	*68.7*	*3.3*	*0.8*	*0.1*	*0.9*	*17.6*	*0.0*	*0.0*	*0.0*	*0.0*	*0.0*	*100.0*	*11.7*
B2	MI	1_3	6.4	0.1	71.7	3.7	0.9	0.2	2.0	14.7	0.1	0.1	0.0	0.0	0.0	100.0	10.1
B2	MI	1_4	5.2	0.1	72.0	5.0	0.5	0.3	2.8	13.5	0.3	0.2	0.0	0.0	0.1	99.9	10.2
Phenocrysts																	
L8bott	feld.	3_1	9.2	0.0	66.2	2.5	1.8	0.0	0.3	20.5	n.a.	n.a.	n.a.	n.a.	0.0	100.5	11.7
B2	cpx	2_1	0.5	8.6	51.7	0.0	20.1	0.2	18.7	0.5	n.a.	n.a.	n.a.	n.a.	1.0	101.4	0.5

All values are in wt.%, Measurements in italics and highlighted green have major element concentrations consistent with partial analysis of a crystal phase. MG = matrix glass; MI = melt inclusion; feld. = feldspar; cpx = clinopyroxene

Table DR6: Major element EPMA data from Dalakvísl matrix glasses, melt inclusions and phenocrysts

Sample name	Material	Analysis number	Na_2O	MgO	SiO_2	K_2O	CaO	TiO_2	FeO	Al_2O_3	F	Cl	SO_2	P_2O_5	MnO	Total	Na_2O+K_2O
Matrix glass																	
D1	MG	2_1	4.9	0.1	73.4	4.6	0.5	0.3	2.4	12.8	0.3	0.1	0.0	0.0	0.1	99.7	9.6
D1	MG	2_2	4.9	0.1	74.0	4.8	0.5	0.3	2.6	13.0	0.3	0.1	0.0	0.0	0.1	100.8	9.7
D1	MG	2_3	4.8	0.2	74.1	4.7	0.5	0.3	2.4	12.9	0.3	0.1	0.0	0.0	0.1	100.5	9.5
D1	MG	O_25	4.4	0.1	72.1	4.5	0.4	0.3	2.1	11.9	0.4	0.1	0.0	0.0	0.1	96.6	8.9
D1	MG	O_26	4.4	0.1	72.0	4.6	0.4	0.3	2.1	11.7	0.3	0.1	0.0	0.0	0.1	96.3	9.0
D1	MG	O_27	4.7	0.2	70.7	4.4	0.4	0.3	2.6	11.5	0.3	0.1	0.0	0.0	0.1	95.4	9.1
D1	MG	O_28	4.5	0.1	73.9	4.7	0.3	0.4	2.5	12.3	0.3	0.1	0.0	0.0	0.1	99.3	9.2
D1	MG	O_29	4.6	0.1	74.0	4.6	0.4	0.4	2.3	12.2	0.3	0.1	0.0	0.0	0.1	99.2	9.2
D13a	MG	O_1	4.9	0.2	74.0	4.3	0.6	0.3	2.1	13.1	0.3	0.1	0.0	0.0	0.1	100.2	9.2
D13a	MG	O_2	5.1	0.2	74.5	4.3	0.5	0.3	2.4	12.9	0.3	0.1	0.0	0.0	0.1	100.7	9.3

D13a	MG	O_3	5.1	0.2	74.4	4.4	0.6	0.3	2.2	13.3	0.2	0.1	0.0	0.0	0.1	101.0	9.4
D13a	MG	O_7	5.0	0.2	74.5	4.2	0.6	0.3	2.6	13.1	0.2	0.1	0.0	0.0	0.2	101.1	9.2
D13a	MG	O_8	4.9	0.2	74.1	4.3	0.5	0.3	2.3	13.0	0.3	0.1	0.0	0.0	0.1	100.3	9.3
D13a	MG	O_9	5.1	0.1	74.5	4.2	0.6	0.3	2.5	13.2	0.3	0.1	0.0	0.0	0.2	101.1	9.3
D13a	MG	O_10	5.0	0.2	74.3	4.1	0.6	0.3	2.4	13.0	0.3	0.1	0.0	0.0	0.2	100.4	9.1
D13a	MG	O_11	5.0	0.2	74.4	4.2	0.5	0.3	2.1	12.9	0.3	0.1	0.0	0.0	0.2	100.2	9.2
D13a	MG	O_12	5.1	0.2	74.3	4.4	0.5	0.3	2.5	13.0	0.3	0.1	0.0	0.0	0.1	100.9	9.4
D13b	MG	2_2	5.1	0.2	74.3	4.3	0.5	0.3	2.4	13.2	0.2	0.1	0.0	0.0	0.1	100.8	9.4
D13b	MG	2_3	5.0	0.2	74.0	4.3	0.5	0.3	2.2	13.1	0.3	0.1	0.0	0.0	0.1	100.1	9.4
D13b	MG	2_4	5.0	0.2	74.3	4.2	0.5	0.4	2.5	13.1	0.3	0.1	0.0	0.0	0.1	100.7	9.2
D13b	MG	2_5	5.1	0.2	74.1	4.4	0.5	0.3	2.6	12.8	0.3	0.1	0.0	0.0	0.1	100.5	9.5
D13b	MG	O_33	5.0	0.2	73.2	4.3	0.5	0.3	2.4	12.9	0.3	0.1	0.0	0.0	0.2	99.4	9.3
D13b	MG	O_34	4.9	0.2	73.2	4.3	0.6	0.3	2.3	12.9	0.3	0.1	0.0	0.0	0.2	99.3	9.2
D13b	MG	O_35	5.0	0.2	73.2	4.2	0.6	0.4	2.6	13.1	0.2	0.1	0.0	0.0	0.1	99.7	9.2
D13b	MG	O_36	5.0	0.1	73.5	4.3	0.5	0.3	2.2	12.9	0.3	0.1	0.0	0.0	0.1	99.5	9.3
D13b	MG	O_37	5.0	0.1	72.9	4.2	0.5	0.3	2.4	12.8	0.3	0.1	0.0	0.0	0.1	98.9	9.2
D13b	MG	O_38	5.1	0.1	72.9	4.3	0.6	0.3	2.5	13.1	0.3	0.1	0.0	0.0	0.1	99.6	9.4
D13b	MG	O_39	5.0	0.2	73.0	4.3	0.6	0.3	2.5	12.9	0.3	0.1	0.0	0.0	0.1	99.4	9.3
D13b	MG	O_40	5.1	0.2	73.7	4.3	0.5	0.3	2.6	13.2	0.3	0.1	0.0	0.0	0.1	100.4	9.4
D13b	MG	O_41	5.0	0.2	73.2	4.4	0.5	0.3	2.4	13.1	0.3	0.1	0.0	0.0	0.1	99.7	9.4
D13b	MG	O_42	5.0	0.1	73.5	4.3	0.5	0.3	2.5	13.1	0.3	0.1	0.0	0.0	0.1	99.9	9.3
D22	MG	2_1	4.8	0.2	74.4	4.9	0.4	0.4	2.4	13.0	0.3	0.1	0.0	0.0	0.1	101.0	9.7
D22	MG	2_2	4.8	0.1	73.9	5.1	0.5	0.3	2.0	13.0	0.3	0.1	0.0	0.0	0.1	100.4	9.9
D22	MG	2_3	4.8	0.2	74.5	4.8	0.5	0.4	2.3	12.9	0.3	0.1	0.0	0.0	0.1	101.0	9.6
D22	MG	2_4	4.9	0.1	74.3	4.8	0.4	0.3	2.3	12.9	0.3	0.1	0.0	0.0	0.2	100.9	9.7
D22	MG	O_16	6.3	0.2	75.3	3.1	0.5	0.4	2.3	13.1	0.2	0.1	0.0	0.0	0.2	101.7	9.4
D22	MG	O_17	6.4	0.1	74.3	3.3	0.5	0.3	2.1	13.3	0.1	0.1	0.0	0.0	0.1	100.6	9.7
D22	MG	O_18	5.3	0.2	74.5	4.3	0.4	0.3	2.2	13.0	0.2	0.2	0.0	0.0	0.2	100.8	9.7
D22	MG	O_19	6.5	0.1	75.8	1.6	0.4	0.4	2.0	13.7	0.0	0.1	0.0	0.1	0.1	100.7	8.0
D22	MG	O_20	6.5	0.2	75.4	1.6	0.5	0.4	3.1	13.5	0.0	0.1	0.0	0.1	0.1	101.5	8.1
D22	MG	O_21	6.6	0.2	72.4	1.9	0.8	0.3	2.8	15.0	0.8	0.1	0.0	0.1	0.2	101.1	8.5
Melt inclusions																	
D1	MI	1_1	4.7	0.2	72.5	4.7	0.5	0.4	2.3	12.9	0.3	0.1	0.0	0.0	0.2	98.8	9.4
D1	*MI*	*1_2*	*8.5*	*0.0*	*68.4*	*2.6*	*1.3*	*0.1*	*1.0*	*17.9*	*0.0*	*0.1*	*0.0*	*0.0*	*0.1*	*100.1*	*11.1*
D1	*MI*	*1_3*	*9.1*	*0.0*	*64.2*	*1.1*	*3.7*	*0.1*	*0.4*	*22.5*	*0.0*	*0.0*	*0.0*	*0.0*	*0.0*	*101.2*	*10.2*
D1	MI	O_22	3.4	0.2	73.1	4.9	0.5	0.4	2.8	11.6	0.2	0.1	0.0	0.0	0.1	97.5	8.4
D1	*MI*	*O_23*	*3.2*	*0.1*	*41.6*	*1.7*	*0.2*	*0.2*	*0.3*	*7.3*	*0.2*	*0.1*	*0.0*	*0.0*	*0.1*	*55.1*	*5.0*
D1	MI	O_24	4.9	0.1	74.4	4.2	0.5	0.4	2.1	11.8	0.2	0.1	0.0	0.0	0.1	98.9	9.1
D13a	MI	1_1	5.0	0.1	72.3	4.1	0.5	0.3	2.5	13.0	0.3	0.1	0.0	0.0	0.1	98.5	9.1
D13a	MI	1_2	4.3	0.2	70.4	4.1	0.5	0.3	2.1	12.8	0.7	0.1	0.0	0.0	0.1	95.8	8.4
D13a	MI	1_3	5.1	0.2	73.7	4.3	0.5	0.3	2.4	12.9	0.2	0.1	0.0	0.0	0.1	100.0	9.4
D13a	MI	O_4	5.1	0.2	74.1	4.3	0.6	0.3	2.3	13.1	0.2	0.1	0.0	0.0	0.1	100.5	9.4
D13a	MI	O_5	5.0	0.2	73.6	4.3	0.6	0.3	2.0	12.8	0.3	0.1	0.0	0.0	0.1	99.3	9.3
D13a	MI	O_6	5.1	0.2	74.4	4.3	0.5	0.3	2.4	12.7	0.2	0.1	0.0	0.0	0.1	100.6	9.5

D13b	*MI*	*1_1*	*8.5*	*0.0*	*62.5*	*1.8*	*2.1*	*0.0*	*0.4*	*23.7*	*0.1*	*0.0*	*0.0*	*0.0*	*0.0*	*99.6*	*10.3*
D13b	MI	1_2	3.9	0.2	72.2	4.1	0.5	0.4	2.2	12.2	0.3	0.1	0.0	0.0	0.1	96.2	8.0
D13b	*MI*	*1_3*	*8.4*	*0.1*	*66.9*	*2.3*	*1.7*	*0.0*	*0.8*	*19.0*	*0.0*	*0.0*	*0.0*	*0.0*	*0.0*	*99.5*	*10.7*
D13b	MI	O_30	4.8	0.2	71.7	4.0	0.5	0.3	2.4	12.7	0.3	0.1	0.0	0.0	0.1	97.3	8.8
D13b	MI	O_31	4.9	0.2	72.1	4.2	0.5	0.3	2.5	12.8	0.3	0.1	0.0	0.0	0.1	98.1	9.1
D13b	MI	O_32	4.9	0.2	71.5	4.2	0.5	0.3	2.3	12.6	0.3	0.1	0.0	0.0	0.1	97.0	9.1
D22	MI	1_1	5.1	0.2	72.1	4.5	0.5	0.4	2.1	12.7	0.3	0.1	0.0	0.0	0.1	98.2	9.7
D22	*MI*	*1_2*	*9.5*	*0.0*	*67.2*	*2.1*	*1.6*	*0.0*	*0.5*	*20.4*	*0.0*	*0.0*	*0.0*	*0.0*	*0.0*	*101.7*	*11.6*
D22	*MI*	*1_3*	*9.6*	*0.0*	*66.2*	*1.5*	*2.4*	*0.0*	*0.4*	*21.2*	*0.0*	*0.0*	*0.0*	*0.0*	*0.0*	*101.7*	*11.1*
D22	*MI*	*O_13*	*9.5*	*0.0*	*66.5*	*1.7*	*2.2*	*0.0*	*0.5*	*20.6*	*0.0*	*0.0*	*0.0*	*0.0*	*0.0*	*101.4*	*11.2*
D22	*MI*	*O_14*	*9.5*	*0.0*	*66.5*	*1.7*	*2.4*	*0.0*	*0.5*	*21.2*	*0.0*	*0.0*	*0.0*	*0.0*	*0.0*	*101.9*	*11.1*
D22	*MI*	*O_15*	*9.5*	*0.0*	*66.6*	*2.0*	*2.0*	*0.0*	*0.5*	*20.7*	*0.0*	*0.0*	*0.0*	*0.0*	*0.0*	*101.5*	*11.5*
Phenocrysts																	
D1	cpx	1_4	0.5	13.7	52.6	0.0	19.6	0.4	11.7	0.8	n.a.	n.a.	n.a.	n.a.	1.5	100.7	0.5
D13b	feld.	2_1	9.1	0.0	65.9	1.9	2.1	0.0	0.5	20.7	n.a.	n.a.	n.a.	n.a.	0.0	100.3	11.0

All values are in wt.%. Measurements in italics and highlighted green have major element concentrations consistent with partial analysis of a crystal phase. MG = matrix glass; MI = melt inclusion; feld. = feldspar; cpx = clinopyroxene

Identifying post-entrapment crystallisation

As melt inclusions cool, post-entrapment crystallisation can occur within the MI which will modify its composition by depleting it in certain elements and enriching the inclusion in incompatible elements such as volatile species (Wallace, 2005). When crystal growth occurs as precipitation on the inclusion/crystal interface it is not visually obvious but due to the modification of MI chemistry it is detectable by EPMA (Webster and Duffield, 1991). We have compared the MI, matrix glass and phenocryst compositions of various samples collected from Bláhnúkur and Dalakvísl. A number of our glass measurements show lower-than-expected silica and erroneously high alkali contents (marked in green and italics in T5 and T6). As these occurrences are particularly common in inclusions, we interpret these as being partial (or complete) analysis of a crystal phase i.e. missed MI or interference from microlites in the case of matrix glass. However, these poorly placed probe points, greatly expand our databank of crystal chemistry and have proved useful in F8.

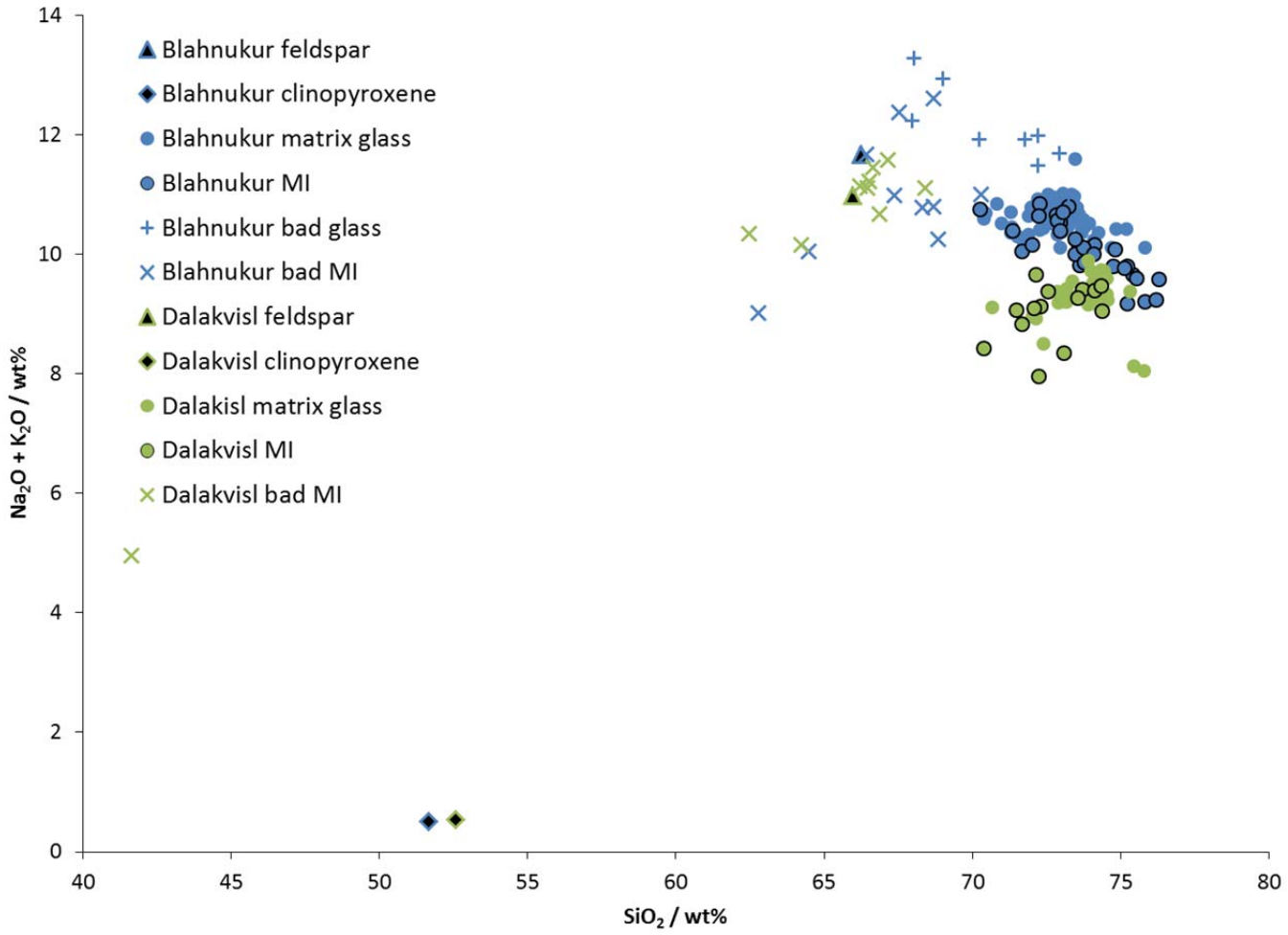

Figure DR8: Total alkali vs silica (TAS) plot of EPMA data for Bláhnúkur (blue) and Dalakvísl (green).

Of the eight Bláhnúkur samples analysed, four (J3, J5, J11 & L6c) contain MIs which are SiO_2-rich and alkali-poor in comparison to the matrix glass (F8). When viewed as individual samples it can be seen that these trends are strongly linear and have crystal (missed MI) measurements as an end member (F9). This trend is consistent with post-entrapment crystallisation of feldspar within the MI. By contrast, the MI from J2b, J10, L8bott and B2 (plus some of the MI from J3 and J5) have major element chemistry that is strongly overlapping with the matrix glass data, suggesting that these MI have not experienced post-entrapment crystallisation. For Bláhnúkur, none of the successful SIMS data was taken from the same MI as EPMA, therefore we cannot state whether or not individual SIMS measurements may be affected by post-entrapment crystallisation. However, we can state that post-entrapment crystallisation is likely in MI from J3 and J11 but unlikely in MI from J2b and L8bott. However, based on the SIMS data, we do not consider H_2O-enrichment to be a significant process in the Bláhnúkur inclusions (section 6.3).

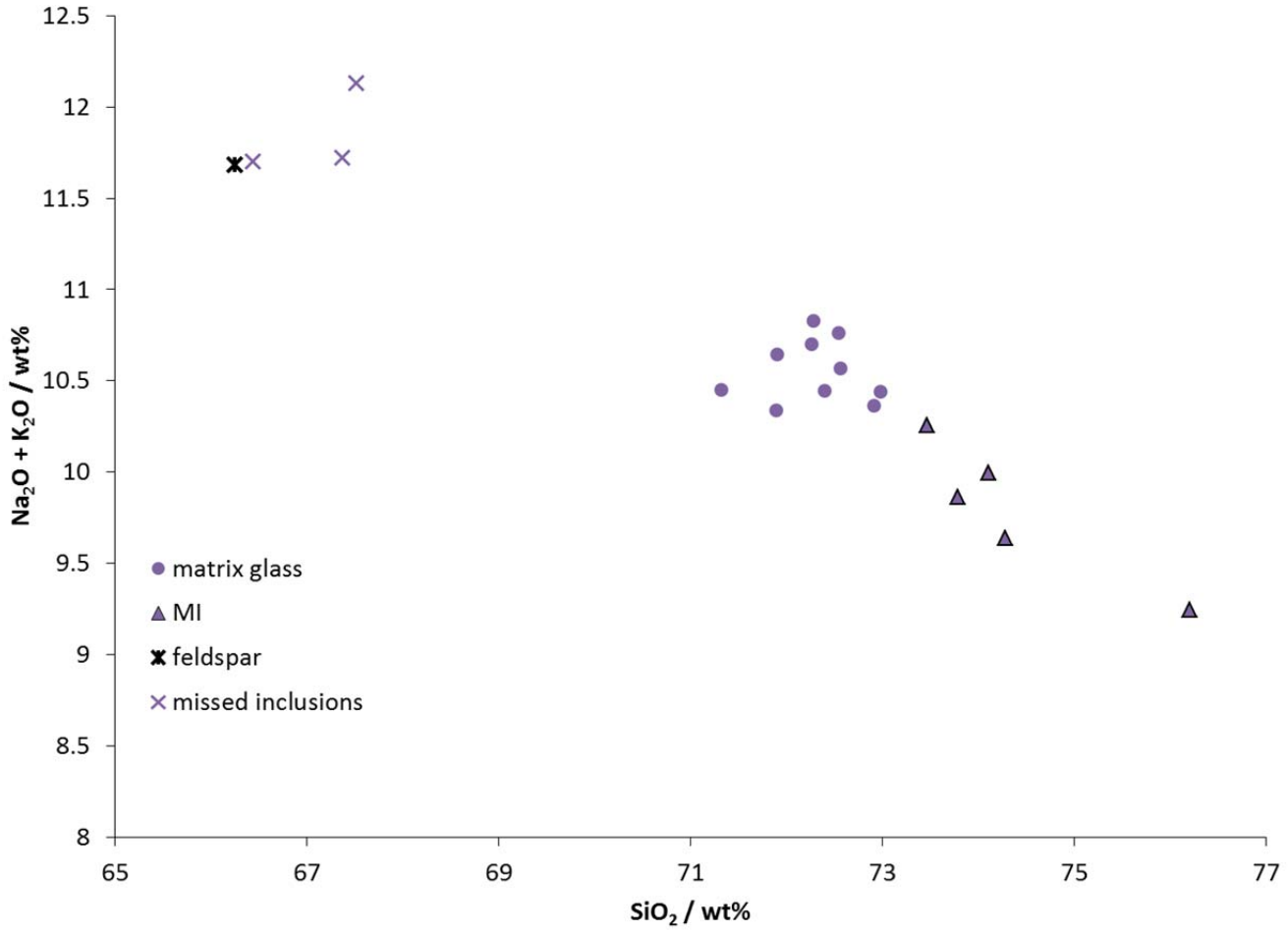

Figure DR9: TAS plot of EPMA data for L6c

The Dalakvísl data paints a very different story to the Bláhnúkur data. In general there is little variation in MI and matrix glass data (F8), the exception being a small number of MI from D13a and D13b. However, unlike the Bláhnúkur MI that have compositions deviating away from that of the phenocryst composition (F9), consistent with post-entrapment crystallisation, the deviating Dalakvísl MI have compositions that are more similar to the phenocryst compositions (F10a). This suggests that the EPMA beam was partially analysing a crystal phase. However, what is interesting is that the deviating Dalakvísl MI, are showing a strong tendency towards clinopyroxene composition (cpx), however, the probed MI were hosted within feldspar. Therefore, either cpx microlites existed in the melt that became trapped to form the MI or there has been crystallisation of cpx within the MI post-entrapment. We have no evidence of the latter as none of the Dalakvísl MI show enrichment in SiO_2 (F8). Furthermore, if cpx had crystallised post-entrapment, we would expect enriched H_2O close to cpx contaminated probe measurements e.g. at points close to 1_1 and particularly 1_2, relative to 1_3 in F10b; however, H_2O concentrations seem relatively homogenous (apart from suspected partial analysis of crystal towards the bottom left inclusion margin). We therefore conclude from our data that it is more likely that any cpx phase within the MI was pre-existing and that even if it did crystallise post-entrapment, there has been neligible enrichment of H_2O.

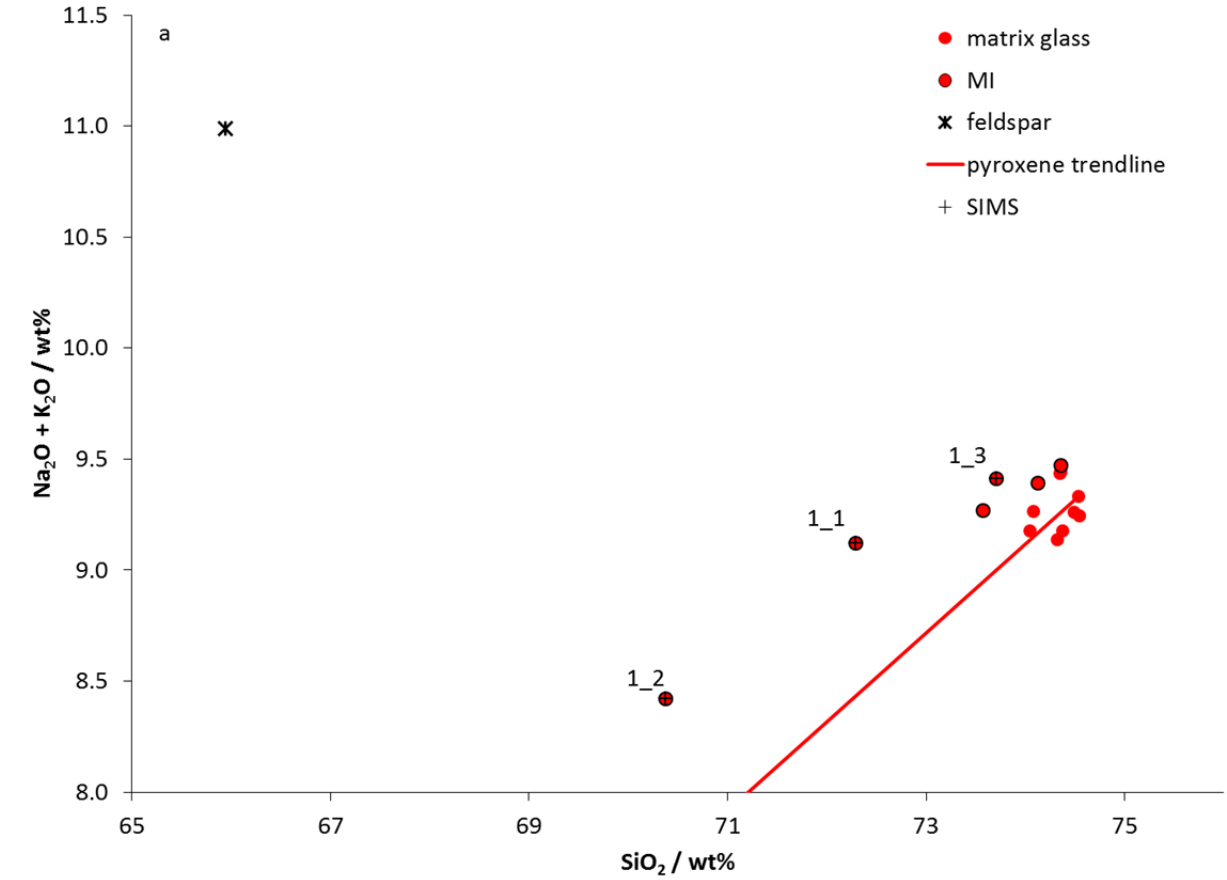

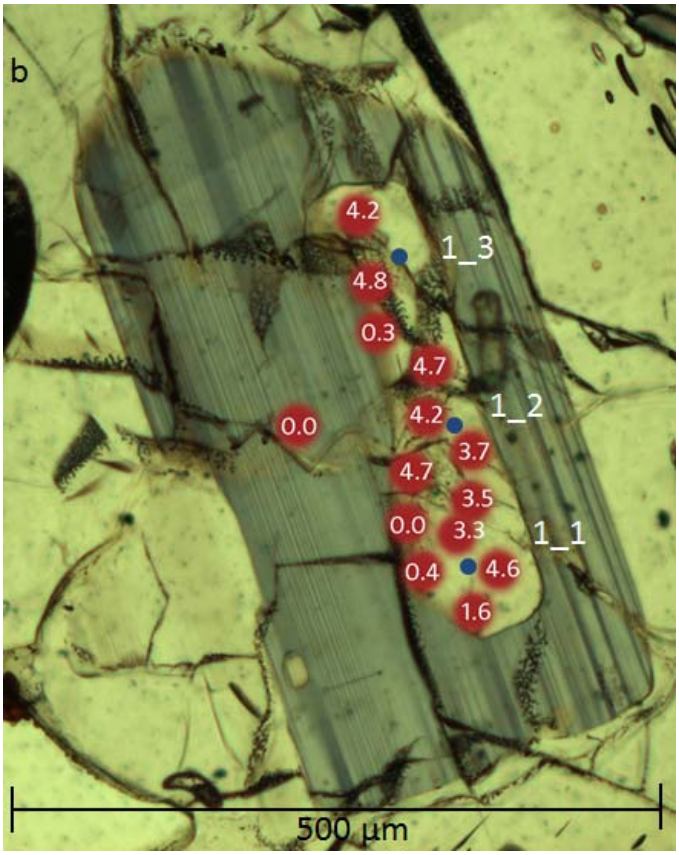

Figure DR10: (a) TAS plot of EPMA data for D13a. The MI data points marked with a plus sign and labelled with their analysis number (T6) were all collected from a single inclusion which is shown in F10b and was also probed using SIMS. The red line connects a typical D13a matrix glass composition with that of the cpx (F8) (b) a photomicrograph mosaic of a feldspar phenocryst in D13a taken in plane-polarised light. There is a large MI in the middle and numerous cracks dissect both the crystal and MI. The blue dots (labelled 1_1, 1_2 and 1_3) mark the location of the EPMA measurements shown in F10a. The red dots mark the locations of SIMS probe-points and the values within them show the measured water contents in wt.% (matrix glass H_2O content is < 1 wt.%).

DR5. SIMS analysis

SIMS Method

We used secondary ion mass spectroscometry (SIMS) to analyse matrix glass and melt inclusions to determine post- and pre- eruptive volatile contents respectively. We analysed H_2O, CO_2, Li, Be, B, F and Cl. This was achieved with the Cameca ims 4f Ion Microprobe at the University of Edinburgh, UK. We used a 5 nA primary beam of 16O-ions to accelerate onto the sample surface. This had a net impact energy of 14.5 keV. Surface contamination was removed with a 2 min pre-sputter with the beam rastered over a ~10 μm square area. The beam size was ~ 14 x 17 μm. Counts were collected over 15 cycles, however, only the last 10 cycles were used in order to further reduce any surface/vacuum background contribution. The background count rate of the electron multiplier detector was monitored using mass 0.7. Prior to each analysis the mass was calibrated for the position of all secondary ions. The internal standard was ^{30}Si. The primary calibration standard for Li, B, F and Cl was the NIST standard SRM610. Rhyolite glass standards were used to calibrate H2O and CO2 which were measured daily. Corrections were made for the overlap of $^{24}Mg^{2+}$ on ^{12}C based on $^{25}Mg^{2+}$ measured at mass 12.5.

To evaluate post-entrapment modification (section 6), inclusion morphology was carefully noted, together with evidence for cracking or bubble formation (T7). Multiple melt inclusions were analysed from multiple phenocrysts (predominantly feldspar but also clinopyroxene) from 14 samples (T1).

We applied careful screening to reject analyses that had unstable counts or low Si counts. T7 shows the data from all analyses that met this screening (87 out of 164 analyses). As can be seen in T7, two samples (R42a and D7b(1)) have matrix glasses with >5 wt.%. We suspect that these samples are hydrated as so we have dismissed them from the dataset (highlighted blue in T7). Furthermore, bubble-containing inclusions tended to display anomalously high Cl and/or H_2O concentrations (T7). Bubbles within MI are often attributed to post-entrapment modification (Lowenstern, 1995) and can form due to volatile enrichment following post-entrapment crystallisation (Steele-MacInnis et al., 2011). Thus bubble-containing inclusions were removed (highlighted orange in T7). Our final data set consisted of 62 analyses, taken from 28 melt inclusions in 10 samples, collected from 5 subglacial rhyolitic edifices within Torfajökull (T7).

The absolute error for SIMS has been estimated at 10%, with the exception of Cl at <20% but relative differences will be significantly less (R. Hinton, 2012, *pers. comm.*).

SIMS results

Table DR7: SIMS data and MI textures, morphologies

Sample name _ analysis number	material	H_2O / wt.%	Cl / ppm	MI shape	MI size / µm	Crack within MI?	Bubble within MI?
A1a							
A1a_MI10_5	matrix glass	0.21	860	n/a	n/a	n/a	n/a
A1a_MI10_2	MI in feld.*	0.27	1092	sv	100	no	no
A1a_MI10_3	MI in feld.	0.30	1556	sv	120	yes	no
A1a_MI10_4	MI in feld.	0.31	1117	sv	130	no	no
A1a_MI9_1	MI in feld.	0.20	1082	rd	20	yes	no
J3							
J3_MI3_5	matrix glass	0.87	1902	n/a	n/a	n/a	n/a
J3_MI3_1	MI in feld.	0.90	2001	sv	60	no	no
J3_MI3_2	MI in feld.	1.04	1998	sv	60	no	no
J3_MI3_4	MI in feld.	0.95	2180	sv	60	yes	no
J3_MI13_1	MI in feld.	1.77	1186	rd	30	no	no
J3_MI13_2	MI in feld.	1.28	2213	rd	50	yes	no
J3_MI5_1	MI in feld.	1.14	2259	sv	100	no	no
J3_MI11_1	*Mi in cpx*	*4.18*	*3459*	*rd*	*50*	*yes*	*yes*
J3_MI3_3	*MI in feld.*	*4.33*	*3307*	*rd*	*60*	*no*	*yes*
J2b							
J2b_MI6_4	matrix glass	0.36	1418	n/a	n/a	n/a	n/a
J2b_MI6_5	MI in feld.	0.43	2638	sv	30	yes	no
J2b_MI7_4	MI in feld.	0.53	2267	sv	40	no	no
J2b_MI7_5	MI in feld.	0.39	1787	sv	40	no	no
J2b_MI4_4	*Mi in cpx*	*1.88*	*2247*	*rd*	*30*	*yes*	*yes*
J11							
J11_MI3_8	matrix glass	0.49	1441	n/a	n/a	n/a	n/a
J11_MI3_1	MI in feld.	0.60	2056	sv	20	yes	no
J11_MI3_6	MI in feld.	0.67	2525	sv	70	no	no
J11_MI3_3	*MI in feld.*	*1.02*	*2301*	*sv*	*30*	*no*	*yes*
L8bott							
L8bott_MI9_6	Matrix glass	0.88	1606	n/a	n/a	n/a	n/a
D1							
D1_MI1_7	matrix glass	1.13	1171	n/a	n/a	n/a	n/a
D1_MI1_1	MI in feld.	1.04	1326	rd	70	yes	no
D1_MI1_3	MI in feld.	0.92	1155	rd	50	yes	no
D1_MI1_4	MI in feld.	2.41	1554	rd	70	yes	no
D1_MI1_5	MI in feld.	1.12	1433	rd	70	yes	no
D1_MI1_2	*MI in feld.*	*1.58*	*1280*	*rd*	*80*	*no*	*yes*
D1_MI2_3	*MI in feld.*	*3.94*	*1493*	*rd*	*60*	*yes*	*yes*

D13a							
D13a_MI1_4	matrix glass	0.92	596	n/a	n/a	n/a	n/a
D13a_MI1_5	MI in feld.	3.29	1106	sv	60	yes	no
D13a_MI6_3	MI in feld.	4.58	1234	rd	220	yes	no
D13a_MI6_4	MI in feld.	1.59	878	rd	220	yes	no
D13a_MI6_5	MI in feld.	3.69	1089	rd	220	yes	no
D13a_MI6_6	MI in feld.	4.19	1184	rd	220	yes	no
D13a_MI6_7	MI in feld.	4.23	1280	rd	220	yes	no
D13a_MI6_8	MI in feld.	4.77	1182	rd	220	yes	no
D13a_MI6_10	MI in feld.	4.71	1169	rd	220	yes	no
D13a_MI6_11	MI in feld.	4.70	1153	rd	220	yes	no
D13a_MI6_12	MI in feld.	3.51	1955	rd	220	yes	no
D13a_MI6_13	MI in feld.	3.30	1092	rd	220	yes	no
D13a_MI1_3	*MI in feld.*	*5.15*	*1358*	*sv*	*130*	*yes*	*yes*
D13a_MI1_7	*MI in feld.*	*2.65*	*974*	*sv*	*40*	*yes*	*yes*
D22							
D22_MI3_13	matrix glass	0.70	885	n/a	n/a	n/a	n/a
D22_MI3_6	MI in feld.	2.88	1942	sv	260	yes	no
D22_MI3_7	MI in feld.	0.78	1225	sv	260	yes	no
D22_MI3_8	MI in feld.	1.75	1493	sv	260	yes	no
D22_MI3_9	MI in feld.	0.81	1428	sv	260	yes	no
D22_MI3_10	MI in feld.	2.45	1834	sv	260	yes	no
D22_MI3_11	MI in feld.	2.67	1675	sv	260	yes	no
D22_MI3_12	MI in feld.	0.77	1254	sv	260	yes	no
D22_MI5_2	MI in feld.	0.64	1224	rd	130	no	no
D22_MI3_19	*MI in feld.*	*2.40*	*2385*	*rd*	*50*	*no*	*yes*
D7b(1)							
D7b(1)_MI1_12		*5.06*	*1058*	*n/a*	*n/a*	*n/a*	*n/a*
D7b(1)_MI1_5	*MI in feld.*	*3.25*	*1075*	*rd*	*40*	*yes*	*yes*
D7b(1)_MI1_1	*MI in feld.*	*5.33*	*1259*	*rd*	*50*	*yes*	*yes*
R7							
R7_MI10_4	matrix glass	0.12	1101	n/a	n/a	n/a	n/a
R7_MI9_1	*Mi in cpx***	*3.16*	*1772*	*rd*	*100*	*no*	*yes*
R7_MI9_2	*Mi in cpx***	*3.07*	*1756*	*rd*	*100*	*no*	*yes*
R7_MI10_1	*MI in feld.*	*0.49*	*1507*	*rd*	*120*	*yes*	*yes*
R7_MI10_2	*MI in feld.*	*0.68*	*1443*	*rd*	*120*	*yes*	*yes*
R13							
R13_MI7_15	matrix glass	0.16	1061	n/a	n/a	n/a	n/a
R13_MI7_4	MI in feld.	3.26	1615	sv	130	yes	no
R13_MI7_5	MI in feld.	1.47	1226	sv	130	yes	no
R24a							
R24a_MI8_6	*matrix glass*	*5.41*	*1021*	*n/a*	*n/a*	*n/a*	*n/a*
R24a_MI6_1	*MI in feld.*	*0.18*	*337*	*sv*	*100*	*no*	*yes*
R20ob							

R20ob_MI1_5	matrix glass	0.12	689	n/a	n/a	n/a	n/a
R20ob_MI6_3	MI in feld.	3.13	1199	sv	50	no	no
R20ob_MI6_4	MI in feld.*	0.80	933	sv	90	yes	no
R20ob_MI6_5	MI in feld.*	2.68	1239	sv	90	yes	no
R20ob_MI6_6	MI in feld.*	3.89	1369	sv	90	yes	no
R20ob_MI6_8	MI in feld.	3.23	1294	sv	40	yes	no
R20ob_MI7_1	Mi in cpx	1.52	1219	rd	80	yes	no
R20ob_MI7_2	Mi in cpx	1.52	1142	rd	80	yes	no
R20ob_MI7_3	Mi in cpx	3.18	1577	rd	80	yes	no
R20ob_MI1_3	Mi in cpx	1.06	824	rd	40	no	no
R20ob_MI6_7	*Mi in cpx*	*1.80*	*919*	*rd*	*20*	*yes*	*yes*
S1e							
S1e_phy07_2	MI in feld.	3.32	1409	rd	100	yes	no
S1e_phy07_3	MI in feld.	0.71	1054	rd	100	yes	no
S1e_phy07_4	MI in feld.	0.76	1143	rd	100	yes	no
S1e_MI6_1	*MI in feld.*	*1.08*	*1466*	*rd*	*60*	*yes*	*yes*
S1e_MI4_3	*MI in feld.*	*0.22*	*945*	*rd*	*220*	*yes*	*yes*
S1e_MI4_4	*MI in feld.*	*0.22*	*1014*	*rd*	*220*	*yes*	*yes*
S1e_MI4_5	*MI in feld.*	*0.21*	*988*	*rd*	*220*	*yes*	*yes*
S1e_MI4_6	*MI in feld.*	*0.21*	*1011*	*rd*	*220*	*yes*	*yes*

Measurements in italics have been dismissed, due to either the matrix glass being hydrated (> 5 wt.% - see section 3.5) or due to the presence of a bubble within the MI, and highlighted blue and orange respectively. feld. = feldspar; cpx = clinopyroxene; * = trapped by cpx; ** trapped with iron nodule; sv = sievy / hourglass / leaked morphology; rd = round (unleaked) morphology. Note that L8bott and R7 matrix glasses have not been included in Fig. 2 of paper because L8bott produced no successful MI analysis and all R7 MI contain bubbles

Large MI (T7) allowed for multiple analyses which was important for testing homogeneity but could introduce bias. In F11 we have selected the highest H_2O measurement from each MI and plotted frequency per edifice. F11 demonstrates without bias, that there is systematic variation between edifices and a strong correlation between explosivity and H_2O content.

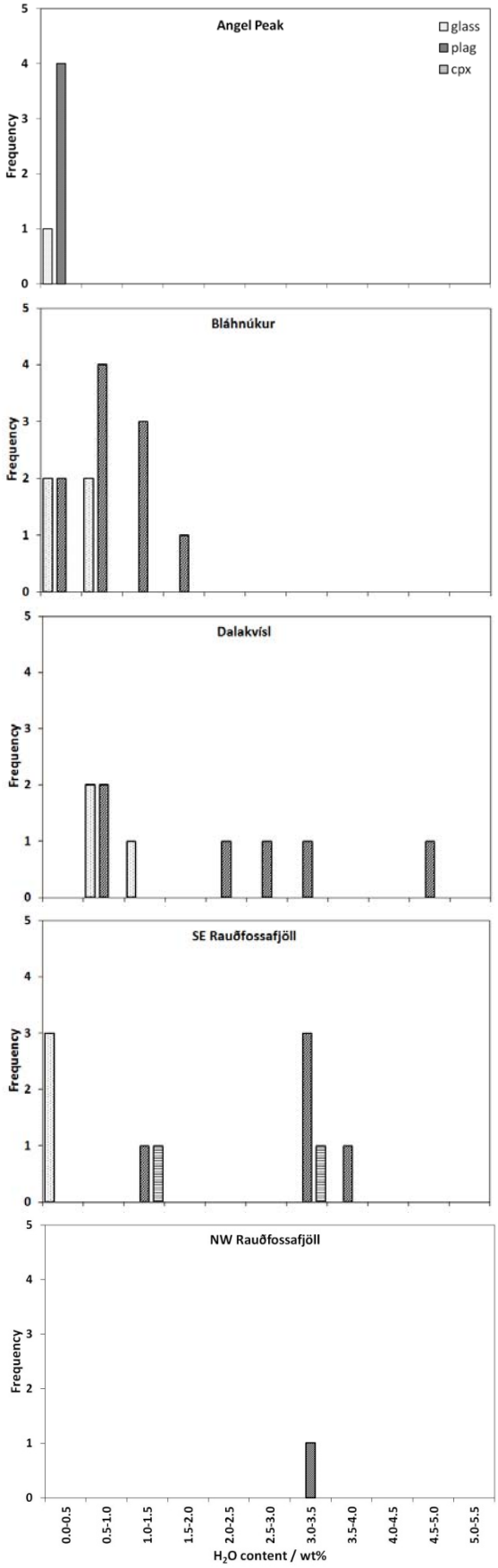

Figure DR11: Frequency graphs showing the highest H_2O content from each MI

Modelling degassing paths

Open- and closed- system degassing can be modelled (Eqs 2&3) using H_2O-Cl relationships (Villemant and Boudon, 1998; Villemant et al., 2008; Humphreys et al., 2009). In a closed-system, the volatiles will remain in the melt. Buoyancy from the volatile phase aids the rise of magma (Ochs and Lange, 1999) and therefore it is generally considered that there is insufficient time for microlite growth during the rapid ascent associated with closed-system degassing (Martel et al., 1998; Villemant et al., 2008). Thus, the expected dissolved chlorine content (Cl^m) for a given dissolved water content can be determined using

$$Cl^m = Cl^0/[1 + D_{Cl}(X_{H2O^0} - X_{H2O^m})] \quad (2)$$

Where Cl is the concentration of chlorine in ppm, D_{Cl} is the chlorine distribution ratio, X is mass fraction of water, superscript '0' refers to initial values and superscript 'm' refers to melt concentrations.

During open-system degassing, a vapour phase segregates from the melt and leaves the system. Some crystallisation is expected in response to H_2O loss (Villemant et al., 2003; Villemant et al., 2008). Thus we shall adopt the formula

$$Cl^m = Cl^0 F^{\Delta^i} \quad (3a)$$

Where $F = 1 - (X_{H2O^0} - X_{H2O^m})(1 + k_{sv})$ (3b)

And $\Delta^i = \frac{D_{Cl}}{1+k_{sv}} - 1$ (3c)

k_{sv} is the mass ratio of crystallising melt to exsolving vapour. Its value depends on initial H_2O content and eruption dynamics, and will increase as degassing and crystallisation take place (Villemant et al., 2003; Villemant et al., 2008; Humphreys et al., 2009). However, for the simplicity of modelling we used constant values and assigned a K_{sv} value of 12 for our water-rich explosive samples; consistent with Humphreys et al. (2009) and Villemant et al. (2008) and a K_{sv} value of 40 for our water-poor effusive samples consistent with Villemant et al. (2003) and Villemant et al. (2008).

The chlorine distribution ratio is defined as wt.% Cl in fluid/wt.% Cl in melt and denoted as D_{Cl}. It is highly composition-sensitive and changes with pressure, temperature, degassing and crystallisation (Webster and Holloway, 1988; Shinohara et al., 1989; Metrich and Rutherford, 1992; Webster, 1992b, a; Signorelli and Carroll, 2000; Webster and De Vivo, 2002; Villemant et al., 2003; Villemant et al., 2008). In rhyolitic melts $1 < D_{Cl} < 170$ (Webster and Holloway, 1988; Shinohara et al., 1989; Webster, 1992b) but if a Cl-rich brine is produced Harford et al. (2003) speculate that D_{Cl} values up to 300 may be possible.

Each edifice seems to show clear and distinct H_2O-Cl relationships, with the exception of Dalakvísl, which seems to have two H_2O-Cl trends attributable to its bimodal behaviour. In each case, we assigned what we attributed to be representative 'initial' H_2O and Cl contents, as displayed in Fig. 2. We then modelled open- and closed- system degassing, using K_{sv} values of 40 and 12 (for effusive and explosive samples respectively), and experimented with various D_{Cl} values, until we found the best fit to our data. These D_{Cl} values are shown on Fig. 2 in the paper.

Post-entrapment modification & identification of unrepresentative melt inclusions

It is possible that MI may be recording non-initial conditions (section 6.1.) or unrepresentative melt (section 6.2.). Furthermore, the composition and volatile content of MI can be modified post-entrapment. There are two principal ways that post-entrapment processes can significantly increase volatile contents within melt inclusions. H diffusion into the melt inclusions can be ruled out because for a given edifice, the matrix glass data is always water-poor by comparison (T7). The other enriching process is post-entrapment crystallisation which shall be discussed in section 6.3. There are also

a number of ways that MI can be depleted in H_2O such as through the formation of a 'shrinkage' bubbles (section 6.4.), MI leaking (section 6.5.) diffusive transfer (section 6.6.) and re-equilibration (section 6.7.) (Lowenstern, 1995).

In this section we show how our sampling and data processing techniques have served to minimise interpretive analysis of modified or unrepresentative MI.

Not initial

MI will not represent 'initial' volatile contents if they were encapsulated once degassing and/or crystallisation had begun (Anderson, 1974; Wallace et al., 1999). With the latter being an inevitable process associated with the capturing of melt inclusions, it questions whether any MI can truly record initial conditions. Nevertheless, MI that contained microlites were not analysed and bubble bearing MI were removed from the data set. Furthermore, every successful measurement within this study reveals that, for a given edifice, melt inclusions are more water-rich than matrix glass (T7), thus we can be confident that the melt-inclusion data in Fig. 2 of the paper, if not recoding 'initial' water contents, are at least giving us insight into pre-eruptive values.

Unrepresentative melt

As crystals grow, they will enrich the surrounding melt in incompatible elements and deplete it in other elements. This is called the 'boundary layer effect' and the encapsulated melt may include this unrepresentative zone (Roedder, 1984; Wallace et al., 1999; Wallace, 2005). However, the effect on H_2O content is relatively small due to its high diffusion coefficient (Baker, 2008). Furthermore Lu et al. (1995) found MIs > 50 µm to be unaffected by the boundary layer effect. As the vast majority of our MIs are > 50 µm (T7), we also consider our data to be representative.

Post-entrapment crystallisation

If crystallisation occurs within the inclusion post-entrapment it will deplete the MI of compatible elements and enrich it in incompatible elements such as volatiles (Wallace, 2005; Steele-MacInnis et al., 2011). Crystallisation within MI tends to begin with precipitation of a crystal phase at the MI-crystal phase boundary (Lowenstern, 1995). This precipitation is not always visible (Webster and Duffield, 1991), however, a bubble may form if there is significant enough enrichment though crystallisation (Steele-MacInnis et al., 2011), thus we removed bubble bearing MI from the database (T7). Only during slow cooling will daughter minerals grow within the MI (Webster and Duffield, 1991; Lowenstern, 1995; Wallace, 2005; Moune et al., 2012). The rapid quenching of our samples within a subglacial setting should minimise this process (Wallace, 2005; Moune et al., 2012) and microlite bearing inclusions were avoided.

However, as we previously stated, post-entrapment crystallisation can occur with no visual signs. It can however, be detected with a geochemical investigation (Webster and Duffield, 1991). EPMA data suggests that some of the Bláhnúkur samples may have experienced some post-entrapment crystallisation, however, as the Bláhnúkur samples are water-poor by comparison to the other edifices (Fig. 2 in paper) we do not consider volatile enrichment to be a significant process that over-writes the edifice trends – if anything it suggests that Bláhnúkur should be even more water-poor than we measured. SiO_2 enrichment, consistent with post-entrapment crystallisation of feldspar or clinopyroxene (the two main mineral phases within our samples) was absent from Dalakvísl EPMA data, suggesting that post-entrapment crystallisation has played a negligible role here, where our most water-rich inclusions were found (F11). See also section 4.3.

Shrinkage bubbles

Volatiles can be depleted within a MI by formation of a shrinkage bubbles which occurs due to thermal contraction (Lowenstern, 1995), however, we removed MI that contained bubbles from the dataset. It is possible that bubbles have been removed through sample preparation; however, shrinkage bubbles are often partial vacuums (Lowenstern, 1995) and

are generally < 5% volume (Webster and Duffield, 1991; Johnson et al., 1994) so we conclude that H_2O loss through the formation of a shrinkage bubble is a negligible process.

Leaked inclusions

Hourglass inclusions suggest that a prolonged connection once existed with the host magma, allowing it to 'leak' (Anderson et al., 1989; Bacon et al., 1992). The connection may become blocked during crystal growth at a later stage, essentially trapping the inclusion. If different melt-inclusions becomes trapped in this way at different times, then hourglass inclusions can record a time-line of crystallisation and degassing during ascent (Blundy and Cashman, 2005; Blundy et al., 2006). Many of our MI had a sievy or hourglass morphology suggesting leakage (T7) and not surprisingly our hourglass inclusions were generally water-poor compared to round inclusions, however, not all hourglass inclusions were water-poor (T7) and we have included them in the data-set to show a progressive record of degassing.

Diffusive loss of H_2O

During cooling, cracks can form within the host crystal, which may provide a pathway for water to diffuse out of the MI (Webster and Rebbert, 1998). However, we found that a lot of our cracked MI were water-rich (T7); this H_2O could not have diffused into the MI along the crack because matrix glass H_2O levels are always low (T7). Therefore, we have kept cracked inclusions within our database. In general when cracks were present, we probed as far away from the crack as possible. However, one particularly large melt inclusion allowed for multiple analyses and we found no difference between probing on or away from cracks, with H_2O contents consistently being greater than 4 wt% (F10b). The matrix glass H_2O content for this sample was < 1wt.% and the cracks ran through the inclusion to the crystal margins in multiple places. We theorise that this cracking was a relatively late-stage process after which little diffusive loss could occur. It goes to show that cracked inclusions do not necessarily indicate diffusive loss as is commonly anticipated (Johnson et al., 1994; Wallace et al., 1999; Hauri, 2002).

However, diffusive loss can occur not only through cracks but through the host crystal itself (Webster and Holloway, 1988; Wallace et al., 1999; Wallace, 2005; Moune et al., 2012). Cl diffusion is several times slower than water diffusion (Villemant et al., 2008), thus water loss through diffusion may be identified by varied H_2O/Cl ratios (Anderson, 1974). Consequently, loss by diffusion could explain many of the Bláhnúkur and Dalakvísl melt inclusions where H_2O is similar to the matrix glass but Cl is considerably higher. However, diffusive loss of water should not be a significant process in our samples due to rapid quenching (Hauri, 2002) in their subglacial setting and we attribute most of the H_2O-Cl range to show a progressive record of melt-inclusion entrapment during ascent.

Re-equilibration

During slow ascent or magma stalling, it is possible that melt inclusions could re-equilibrate to their ambient setting through diffusion (Wallace et al., 1999; Humphreys et al., 2008). As it is speculated that the effusive samples had a slow ascent rate and open system degassing, it is possible that this allowed for equilibration at lower pressure conditions after some volatiles had degassed and therefore the recording of lower water contents within the melt inclusions.

However, the low diffusivities of plagioclase, and the high viscosity of rhyolite means that H_2O diffusion will be a slow process and thus a very slow ascent rate or magma stalling would be required to allow sufficient time for the re-equilibration of melt inclusions (Humphreys et al., 2008). As all of the eruptions within this study were thought to have been triggered by tholeiitic dykes intersecting the rhyolitic Torfajökull magma chamber (evidence from a minor percentage of tholeiitc inclusions within the rhyolitic products) (McGarvie, 1984; McGarvie et al., 1990), it is likely that the rise speed was sufficiently fast and un-interrupted (i.e. no stalling) so as not to let re-equilibration occur.

References

Anderson, A. T., 1974, Chlorine, Sulfur, and Water in Magmas and Oceans: Geological Society of America Bulletin, v. 85, no. 9, p. 1485-1492.

Anderson, A. T., Newman, S., Williams, S. N., Druitt, T. H., Skirius, C., and Stolper, E., 1989, H_2O, CO_2, Cl, and Gas in Plinian and Ash-Flow Bishop Rhyolite: Geology, v. 17, no. 3, p. 221-225.

Bacon, C. R., Newman, S., and Stolper, E., 1992, Water, Co2, Cl, and F in Melt Inclusions in Phenocrysts from 3 Holocene Explosive Eruptions, Crater Lake, Oregon: American Mineralogist, v. 77, no. 9-10, p. 1021-1030.

Baker, D., 2008, The fidelity of melt inclusions as records of melt composition: Contributions to Mineralogy and Petrology, v. 156, no. 3, p. 377-395.

Blundy, J., and Cashman, K., 2005, Rapid decompression-driven crystallization recorded by melt inclusions from Mount St. Helens volcano: Geology, v. 33, no. 10, p. 793-796.

Blundy, J., Cashman, K., and Humphreys, M., 2006, Magma heating by decompression-driven crystallization beneath andesite volcanoes: Nature, v. 443, no. 7107, p. 76-80.

Denton, J. S., Tuffen, H., Gilbert, J. S., and Odling, N., 2009, The hydration and alteration of perlite and rhyolite: Journal of the Geological Society, v. 166, p. 895-904.

Denton, J. S., Tuffen, H., and Gilbert, J. S., 2012, Variations in hydration within perlitised rhyolitic lavas—evidence from Torfajökull, Iceland: Journal of Volcanology and Geothermal Research, v. 223–224, no. 0, p. 64-73.

Furnes, H., Fridleifsson, I. B., and Atkins, F. B., 1980, Subglacial volcanics - on the formation of acid hyaloclastites: Journal of Volcanology and Geothermal Research, v. 8, no. 1, p. 95-110.

Harford, C. L., Sparks, R. S. J., and Fallick, A. E., 2003, Degassing at the Soufrière Hills Volcano, Montserrat, Recorded in Matrix Glass Compositions: Journal of Petrology, v. 44, no. 8, p. 1503-1523.

Hauri, E., 2002, SIMS analysis of volatiles in silicate glasses, 2: isotopes and abundances in Hawaiian melt inclusions: Chemical Geology, v. 183, no. 1–4, p. 115-141.

Humphreys, M. C. S., Kearns, S. L., and Blundy, J. D., 2006, SIMS investigation of electron-beam damage to hydrous, rhyolitic glasses: Implications for melt inclusion analysis: American Mineralogist, v. 91, no. 4, p. 667-679.

Humphreys, M. C. S., Blundy, J. D., and Sparks, R. S. J., 2008, Shallow-level decompression crystallisation and deep magma supply at Shiveluch Volcano: Contributions to Mineralogy and Petrology, v. 155, no. 1, p. 45-61.

Humphreys, M. C. S., Edmonds, M., Christopher, T., and Hards, V., 2009, Chlorine variations in the magma of Soufrière Hills Volcano, Montserrat: Insights from Cl in hornblende and melt inclusions: Geochimica et Cosmochimica Acta, v. 73, no. 19, p. 5693-5708.

Johnson, M. C., Anderson, A. T., and Rutherford, M. J., 1994, Pre-Eruptive Volatile Contents of Magmas: Volatiles in Magmas, v. 30, p. 281-330.

Leschik, M., Heide, G., Frischat, G. H., Behrens, H., Wiedenbeck, M., Wagner, N., Heide, K., Geißler, H., and Reinholz, U., 2004, Determination of H_2O and D_2O contents in rhyolitic glasses: Physics and Chemistry of Glasses, v. 45, no. 4, p. 238-251.

Lowenstern, J. B., 1995, Applications of silicate-melt inclusions to the study of magmatic volatiles, *in* Thompson, J. F. H., ed., Magmas, Fluids and Ore Deposits, Volume 23, Mineralogical Association of Canada, p. 71-99.

Lu, F., Anderson, A. T., and Davis, A., 1995, Diffusional gradients at the crystal/melt interface and their effect on the composition of melt inclusions: The Journal of Geology, v. 103, p. 591-597.

Martel, C., Pichavant, M., Bourdier, J. L., Traineau, H., Holtz, F., and Scaillet, B., 1998, Magma storage conditions and control of eruption regime in silicic volcanoes: experimental evidence from Mt. Pelée: Earth and Planetary Science Letters, v. 156, no. 1-2, p. 89-99.

McGarvie, D. W., 1984, Torfajökull: A volcano dominated by magma mixing: Geology, v. 12, no. 11, p. 685-688.

McGarvie, D. W., MacDonald, R., Pinkerton, H., and Smith, R. L., 1990, Petrogenetic Evolution of the Torfajökull Volcanic Complex, Iceland II. The Role of Magma Mixing: Journal of Petrology, v. 31, no. 2, p. 461-481.

McGarvie, D. W., Burgess, R., Tindle, A. G., Tuffen, H., and Stevenson, J. A., 2006, Pleistocene rhyolitic volcanism at Torfajökull, Iceland: eruption ages, glaciovolcanism, and geochemical evolution: Jökull, v. 56, p. 57-75.

McGarvie, D. W., Stevenson, J. A., Burgess, R., Tuffen, H., and Tindle, A. G., 2007, Volcano-ice interactions at Prestahnúkur, Iceland: rhyolite eruption during the last interglacial-glacial transition: Annals of Glaciology, v. 45, no. 1, p. 38-47.

Metrich, N., and Rutherford, M. J., 1992, Experimental study of chlorine behaviour in hydrous silicic melts: Geochim. Cosmochim. Acta, v. 56, p. 607-616.

Moune, S., Sigmarsson, O., Schiano, P., Thordarson, T., and Keiding, J. K., 2012, Melt inclusion constraints on the magma source of Eyjafjallajökull 2010 flank eruption: J. geophys. Res., v. 117, p. B00C07.

Newman, S., Stolper, E. M., and Epstein, S., 1986, Measurement of water in rhyolitic glasses: calibration of an infrared spectroscopic technique: American Mineralogist, v. 71, no. 11-12, p. 1527-1541.

Ochs, F. A., and Lange, R. A., 1999, The Density of Hydrous Magmatic Liquids: Science, v. 283, no. 5406, p. 1314-1317.

Owen, J., Tuffen, H., and McGarvie, D. W., 2012, Using dissolved H_2O in rhyolitic glasses to estimate palaeo-ice thickness during a subglacial eruption at Bláhnúkur (Torfajökull, Iceland): Bulletin of Volcanology, v. 74, no. 6, p. 1355-1378.

Roedder, E., 1984, Fluid inclusions: an introduction to studies of all types of fluid inclusions, gas, liquid, or melt, trapped in materials from earth and space, and their application to the understanding of geologic processes, Mineralogical Society of America.

Shinohara, H., Iiyama, J. T., and Matsuo, S., 1989, Partition of chlorine compounds between silicate melt and hydrothermal solutions: I. Partition of NaCl-KCl: Geochimica et Cosmochimica Acta, v. 53, no. 10, p. 2617-2630.

Signorelli, S., and Carroll, M. R., 2000, Solubility and fluid-melt partitioning of Cl in hydrous phonolitic melts: Geochimica et Cosmochimica Acta, v. 64, no. 16, p. 2851-2862.

Steele-MacInnis, M., Esposito, R., and Bodnar, R. J., The effect of post-entrapment crystallization on the H_2O and CO_2 concentrations of rhyolitic (silica-rich) melt inclusions, and implications for magma degassing paths, *in* Bakker, R. J., Baumgartner, M., and Doppler, G., eds., Proceedings European Current Research on Fluid Inclusions (ECROFI-XXI), Montanuniversität Leoben, Austria, 2011: Wien, Geologische Bundesanstalt, p. 188-189.

Stevenson, J. A., Gilbert, J. S., McGarvie, D. W., and Smellie, J. L., 2011, Explosive rhyolite tuya formation: classic examples from Kerlingarfjöll, Iceland: Quaternary Science Reviews, v. 30, no. 1-2, p. 192-209.

Tuffen, H., Gilbert, J., and McGarvie, D., 2001, Products of an effusive subglacial rhyolite eruption: Bláhnúkur, Torfajökull, Iceland: Bulletin of Volcanology, v. 63, no. 2, p. 179-190.

Tuffen, H., McGarvie, D. W., Gilbert, J. S., and Pinkerton, H., 2002a, Physical volcanology of a subglacial-to-emergent rhyolitic tuya at Rauðufossafjöll, Torfajökull, Iceland, *in* Smellie, J. L., and Chapman, M. G., eds., Volcano-Ice interaction on Earth and Mars, Volume Special Publication No. 202: London, The Geological Society, p. 213-236.

Tuffen, H., Pinkerton, H., McGarvie, D. W., and Gilbert, J. S., 2002b, Melting of the glacier base during a small-volume subglacial rhyolite eruption: evidence from Bláhnúkur, Iceland: Sedimentary Geology, v. 149, no. 1-3, p. 183-198.

Tuffen, H., McGarvie, D. W., and Gilbert, J. S., 2007, Will subglacial rhyolite eruptions be explosive or intrusive? Some insights from analytical models: Annals of Glaciology, v. 45, no. 1, p. 87-94.

Tuffen, H., McGarvie, D. W., Pinkerton, H., Gilbert, J. S., and Brooker, R. A., 2008, An explosive-intrusive subglacial rhyolite eruption at Dalakvísl, Torfajökull, Iceland: Bulletin of Volcanology, v. 70, no. 7, p. 841-860.

Tuffen, H., Owen, J., and Denton, J., 2010, Magma degassing during subglacial eruptions and its use to reconstruct palaeo-ice thicknesses: Earth-Science Reviews, v. 99, no. 1-2, p. 1-18.

Villemant, B., and Boudon, G., 1998, Transition from dome-forming to plinian eruptive styles controlled by H2O and Cl degassing: Nature, v. 392, no. 6671, p. 65-69.

Villemant, B., Boudon, G., Nougrigat, S., Poteaux, S., and Michel, A., 2003, Water and halogens in volcanic clasts: tracers of degassing processes during Plinian and dome-building eruptions, *in* Oppenheimer, C., Pyle, D. M., and Barclay, J., eds., Volcanic Degassing, Geological Society London, Special Publications, Volume 213, p. 63-79.

Villemant, B., Mouatt, J., and Michel, A., 2008, Andesitic magma degassing investigated through H(2)O vapour-melt partitioning of halogens at Soufriere Hills Volcano, Montserrat (Lesser Antilles): Earth and Planetary Science Letters, v. 269, no. 1-2, p. 212-229.

Walker, G. P. L., 1981, Characteristics of 2 Phreatoplinian Ashes, and Their Water-Flushed Origin: Journal of Volcanology and Geothermal Research, v. 9, no. 4, p. 395-407.

Wallace, P. J., 2005, Volatiles in subduction zone magmas: concentrations and fluxes based on melt inclusion and volcanic gas data: Journal of Volcanology and Geothermal Research, v. 140, no. 1–3, p. 217-240.

Wallace, P. J., Anderson, A. T., Jr., and Davis, A. M., 1999, Gradients in H_2O, CO_2, and exsolved gas in a large-volume silicic magma system: Interpreting the record preserved in melt inclusions from the Bishop Tuff: Journal of Geophysical Research, v. 104, no. B9, p. 20097-20122.

Webster, J. D., 1992a, Fluid-melt interactions involving Cl-rich granites: Experimental study from 2 to 8 kbar: Geochimica et Cosmochimica Acta, v. 56, no. 2, p. 659-678.

Webster, J.D., 1992b, Water solubility and chlorine partitioning in Cl-rich granitic systems: effects of melt composition at 2Kbar and 800°C: Geochimica et Cosmochimica Acta, v. 56, p. 679-687.

Webster, J. D., and De Vivo, B., 2002, Experimental and modeled solubilities of chlorine in aluminosilicate melts, consequences of magma evolution, and implications for exsolution of hydrous chloride melt at Mt. Somma-Vesuvius: American Mineralogist, v. 87, no. 8-9, p. 1046-1061.

Webster, J. D., and Duffield, W. A., 1991, Volatiles and lithophile elements in Taylor Creek Rhyolite; constraints from glass inclusion analysis: American Mineralogist, v. 76, no. 9-10, p. 1628-1645.

Webster, J. D., and Holloway, J. R., 1988, Experimental constraints on the partitioning of Cl between topaz rhyolite melt and H2O and H2O + CO2 fluids: New implications for granitic differentiation and ore deposition: Geochimica et Cosmochimica Acta, v. 52, no. 8, p. 2091-2105.

Webster, J. D., and Rebbert, C. R., 1998, Experimental investigation of H_2O and Cl-solubilities in F-enriched silicate liquids; implications for volatile saturation of topaz rhyolite magmas: Contributions to Mineralogy and Petrology, v. 132, no. 2, p. 198-207.